Check for updates

Utilizing surface modified poultry feathers for senary multi-metal water purification: kinetic and thermodynamic behavior of heavy metal–laden biosorbent†

Muhammad Faisal Irfan, [ab] Tariq Siddique‡*[a] and Aman Ullah ⓘ §*[b]

This study optimized poultry feathers (PFs) in two steps to remove six trace metals (Cr^{6+}, As^{3+}, V^{5+}, Co^{2+}, Ni^{2+}, Cd^{2+}) from contaminated water and evaluated the spent biosorbent's thermal and energy potential. PFs were surface-modified with tetrahydrofuran (THF) and optimized *via* response surface methodology. Optimal pre-treatment (30 °C, 47 min, 0.015 g ml^{-1}) and biosorption (0.17 g, 0.5 h) conditions improved removal of Co^{2+} (+31.5%), Ni^{2+} (+19.5%), Cd^{2+} (+0.6%), and V^{5+} (+6.1%), but reduced Cr^{6+} (−24.1%) and As^{3+} (−1.8%). Thermogravimetric analysis showed higher activation energies for spent biosorbent, with diffusion-controlled degradation confirmed by Coats−Redfern analysis. This dual optimization enhances metal removal and supports scalable bioenergy recovery.

1   Introduction

Currently, the presence of heavy metal-contaminated wastewater poses a significant threat both to the global environment and the well being of humans. This issue stems from the activities of various industries, such as milling, plastics, surface mining, metallurgical processes, electroplating and pigments which contribute to the pollution of water resources.[1,2] One notable example is oil sands process-affected water (OSPW), a byproduct produced during the extraction and processing of bitumen from oil sands, mainly through hot water separation techniques. This wastewater contains a complex blend of organic and inorganic pollutants, such as naphthenic acids, salts (ions like Na^+, Mg^{2+}, Ca^{2+}, SO_4^{2-}, and HCO_3^-), and heavy metals, making it toxic and unsuitable for direct release into the environment. Given the large quantities generated and the environmental hazards involved, managing and treating OSPW effectively has become a major challenge.[3]

Heavy metals, known for their carcinogenic and toxic properties, are non-biodegradable and tend to accumulate in human body and food chains, resulting in health disorders and numerous diseases in living organisms, including humans.[3,4] Efforts to ensure a healthy and clean environment necessitate the removal of even trace amounts of heavy metals from water resources. Biosorption technique emerges as a more viable option for heavy metals elimination from industrial wastewater, due to its cost-effectiveness, minimal energy requirements, superior selectivity, high biosorption efficiency, and the capability to use waste as adsorbent material, resulting in non-toxic by-products.[5–8] Several studies in literature have explored biosorption for removing different heavy metals from contaminated (synthetic) water. However, these studies predominantly depend on conventional techniques, employing a one-factor-at-a-time approach which requires a high number of experiments and overlook interaction effects within input parameters, to optimize multivariable systems or single/binary component systems using a response surface methodology (RSM).[9–11] Considering the complex nature of real-world scenarios, where contaminated water often contains multi-metals, there exists a significant gap that necessitates more rigorous and in-depth investigations. Consequently, a comprehensive understanding of these intricate systems is crucial to address this research gap.

Despite several advantages, biosorption poses a risk of secondary pollution if the spent adsorbents are not properly disposed of. Unlike organic pollutants, heavy metals cannot be degraded or mineralized for safe disposal, making the management of adsorbent waste a challenge. The spent adsorbents have been repurposed in various applications in literature, which include catalysis,[12,13] energy production,[14] forensics,[15] brick and

aDepartment of Renewable Resources, University of Alberta, Edmonton, AB, T6G 2E3, Canada. E-mail: tariq.siddique@ualberta.ca; Fax: +1 (780)492 4323; Tel: +1 (780) 492 2899

bDepartment of Agriculture Food and Nutritional Science, University of Alberta, Edmonton, AB, T6G 2P5, Canada. E-mail: ullah2@ualberta.ca; Fax: +1 (780) 492 4265; Tel: +1 (780) 492 4845

† Electronic supplementary information (ESI) available. See DOI: https://doi.org/10.1039/d5ra02131f

‡ Current address: University of Alberta, 348 F South Academic Building, Edmonton, Alberta T6G 2G7, Canada.

§ Current address: University of Alberta, 360C South Academic Building, Edmonton, Alberta T6G 2G7, Canada.

ceramic manufacturing,[16,17] glass production,[18] and sensor materials.[19] However, these current utilization methods are limited, and there is a need to explore additional ways and applications for managing and using spent adsorbents more effectively. Thermochemical conversion through pyrolysis presents an alternative method where biomass is converted into valuable energy products such as biochar, biooil, and biogas.[20] These products hold significant market potential and can be further refined to meet specific needs. Various studies on pyrolysis of different biomass types, such as bambusa textile,[21] date palm,[22] picual olive pomace,[23] rice husk,[24] mustard stalk,[25] coffee husk,[24] and nutshell[24] have shown promising results for bioenergy production and the determination of kinetic parameters, which are crucial for design and scaling purposes.[26] Poultry feather (parent, spent) is one of the biomasses which contains mainly keratin protein with high carbon and nitrogen content due to the presence of amino acids. Furthermore, the biooil derived from PFs is rich in amino acids, which can be used in various applications as pesticides and fertilizers.[27] Additionally, the biochar produced from PFs contains graphitic nitrogen groups within carbon structures, which can enhance electrocatalytic performance,[28] improving soil fertility,[28] serving as a hydrogen storage material,[29] aiding the synthesis of graphitic carbon for polymer nanocomposites,[28] and being suitable for CO_2 uptake and supercapacitors (Scheme 1).[30]

Although various studies have been conducted on the thermochemical conversion of biomasses, including chicken feathers (CFs), the bioenergy potential and mechanistic aspects (such as kinetics and thermodynamic parameters) of spent PFs have not been explored in the literature, to the best of our knowledge. Therefore, this research first prepares the spent biosorbent containing six heavy metals through the biosorption process and then examines its thermal behavior, kinetic mechanisms, thermodynamic parameters, and bioenergy potential. For biosorption study (biosorbent preparation), we present a statistical dual-optimization framework that addresses both single and multi-objective scenarios, incorporating desirability functions (composite and individual) for independent variables affecting the removal of three oxyanions (V^{5+}, As^{3+}, Cr^{6+}) and three cations (Co^{2+}, Ni^{2+}, Cd^{2+}) from simulated water at a pH of 7.5. These oxyanions and cations were selected for their high toxicity and concentrations in OSPW, as our biosorption study aims to treat OSPW. The optimization process unfolds in two stages to maximize the removal of these trace metals. The first stage, which involves pretreatment of PF, uses RSM with Box–Behnken Design (BBD), while the second stage focuses on process parameters, employing RSM with Central Composite Design (CCD). Independent variables such as pretreatment temperature, pretreatment time, and the PF : THF ratio are adjusted in the first stage, while the second stage examines PF dosage and biosorption time. The removal efficiencies of all trace metals serve as the output responses. Six separate quadratic regression models were developed for each response across both stages, exploring interactions between multiple factors. The significance of all terms, including factors, models, and interactions, was thoroughly analyzed to ensure robust, reliable, and accurate results.
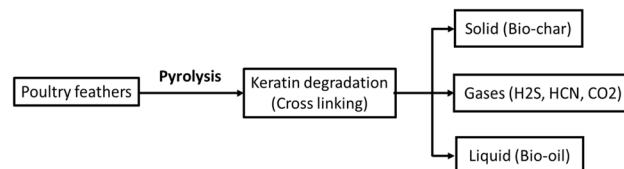
Scheme 1 Thermochemical (pyrolysis) reaction pathway of poultry feathers.

Following the biosorption process, the spent biosorbent (OPT2-ads) was utilized for waste valorization, a promising approach that supports circular economic strategies. We examined an in-depth analysis of thermal decomposition, physicochemical characterization, thermodynamic parameters ($\Delta H^{\neq}$, $\Delta G^{\neq}$, $\Delta S^{\neq}$), and kinetic parameters (activation energy, pre-exponential factor) using TGA data at various heating rates (5, 10, 20, 30 °C min^{-1}) on OPT2-ads and parent PF samples. We applied two established, model-free iso-conversional methods including differential (Friedman), and integral (Kissinger-Akahira-Sunose: KAS). To determine the reaction mechanism and identify the rate-determining step, we evaluated eleven different integral expressions using the well-known Coats–Redfern method. This unique aspect of our work brings novelty, as no available literature comprehensively evaluates the pyrolysis reaction kinetics of OPT2-ads biosorbent, a critical consideration for design and scale-up purposes, offering valuable insights into enhancing biosorption efficiency and its application in large-scale water treatment systems.

2 Experimental

2.1 Materials

The PFs were provided by Sofina Foods, Edmonton, Canada. The feathers were cleaned, dried, and ground as per our previous studies.[3,31] Briefly, PFs were thoroughly washed several times with hot soapy water, then air-dried in a closed fume hood for one to two weeks to ensure complete moisture evaporation. The dried PFs were subsequently ground using a Fritsch cutting mill (Pulverisette 15, Laval Lab Inc., Laval, Canada) equipped with a 0.25 mm sieve insert. The cleaned PFs were then surface modified by THF solvent at different conditions and then stored in a desiccator at ambient temperature. Tetrahydrofuran (purity: 99.8%) as a solvent for the pre-treatment of PFs was obtained from Sigma Aldrich. Three cations and three oxyanions were selected for the adsorption study and their salts were used for their individual stock solutions as follows: cadmium (Cd^{2+}) chloride (Sigma Aldrich 99.9%), nickel (Ni^{2+}) chloride hexahydrate (Fisher Scientific, 99.4%), chromium (Cr^{6+}) oxide (Sigma Aldrich 99.99%), cobaltous (Co^{2+}) sulfate heptahydrate (Fisher Scientific, 100%), and arsenic (As^{3+}) sodium meta arsenite (Sigma Aldrich ≥99%). However, for vanadium (V^{5+}), liquid standard vanadium solution [CAS No: HNO_3 7697-37-2, V 7440-62-2 (SpexCertiPrep)] was used.

2.2 Procedure for the PF surface modification

Surface modification of PF was done in a 500 ml capacity two-neck round bottom flask, using THF as the solvent. The

purpose of treating PF with THF is to eliminate impurities and enhance the physicochemical properties of the PF. This treatment could also help to reveal additional functional groups, thereby improving the biosorption capabilities of PFs. A water cooled condenser was connected to one neck to avoid the loss of solvent during evaporation and a thermometer was attached to another neck to measure the actual reaction temperature. Stirring was maintained at 500 rpm using a magnetic to ensure continuous mixing of the sample with the solvent. To heat the flask, a temperature controlled heat jacket with stirrer was used. PFs were modified under different set of conditions as given in Table 1. Initially, the desired solvent was added to the flask and heated to the required temperature. Once the reaction temperature was achieved, the desired amount of PF was added for the required time as depicted in Table 2. After reaction, the samples were then filtered and dried for 24 h in a fumehood under atmospheric condition. The prepared modified PF samples were then used for the biosorption study *i.e.* pretreatment of PF (Optimization-1).

2.3 Procedure for the removal of metals by biosorption

Simulated wastewater with three cations (Ni^{2+}, Co^{2+}, Cd^{2+}) and three oxyanios (V^{5+}, As^{3+}, Cr^{6+}) each having concentration of 100 $\mu g\ L^{-1}$ was prepared as discussed in our previous studies.[3,31] This simulated waste water is designed as multi-metals

simulated water (MMSW). For Optimization-1, all adsorption experiments (batch) were performed using conical tubes (15 ml) with 0.1 g of modified PF in a 10 ml of MMSW. Conical tubes were placed on a reciprocating shaker for incubation time of 24 h at a constant pH of 7.5. Triplicate experiments were performed, and their average values were used to optimize the pretreatment parameters of PF in Optimization-1. For Optimization-2 *i.e.* process parameter biosorption optimization, PF samples were prepared at the optimal set of conditions obtained from Optimization-1. Afterward, the same biosorption procedure was adopted *i.e.* placing the triplicate conical tubes on the reciprocating shaker with 10 ml of MMSW at a constant pH of 7.5 except the dose of PF and biosorption time as depicted in Table 2. Again, the average values were used to optimize the biosorption process parameters in Optimization-2.

2.4 Two-step optimization using RSM

The purpose of two-step optimization was to maximize the removal efficiencies of trace metals from MMSW using surface modified bio-sorbent. A well-known RSM approach was used for the two-step optimization *i.e.*, pretreatment of PF (Optimization-1) followed by the biosorption process parameters optimization (Optimization-2). For Optimization-1, RSM with BBD having three independent factors *i.e.*, pretreatment temperature (°C), pretreatment time (min) and PF : THF ratio (g

Table 1 Coded levels of each factor with actual values for both optimizations

Optimization 1-(BBD)	Parameter levels			−1	0	+1	
	Process temperature (°C)			25	45	65	
	Process time (min)			5	30	60	
	PF : THF ratio (g ml^{-1})			0.02	0.01	0.0067	
Optimization 2-(CCD)	Parameter levels	−1.414	−1	0	+1	+1.414	
	Dose of PF (g)	0.02	0.055	0.11	0.15	0.2	
	Biosorption time (h)	0.5	1.5	3	4.5	6	

Table 2 Total number of experiments for both optimizations (actual values are in paranthesis)

Optimization-1				Optimization-2		
	Temp (°C)	Time (min)	Ratio (g ml^{-1})		Dose (g)	Time (h)
Runs	Coded (actual) values			Runs	Coded (actual) values	
1	−1 (RT)	−1 (5)	0 (0.01)	1	0 (0.11)	0 (3)
2	0 (45)	1 (60)	1 (0.0067)	2	−1.414 (0.02)	0 (3)
3	1 (65)	0 (30)	1 (0.0067)	3	−1 (0.055)	−1 (1.5)
4	0 (45)	1 (60)	−1 (0.02)	4	0 (0.11)	0 (3)
5	0 (45)	0 (30)	0 (0.01)	5	−1 (0.055)	1 (4.5)
6	1 (65)	−1 (5)	0 (0.01)	6	1 (0.15)	1 (4.5)
7	−1 (RT)	1 (60)	0 (0.01)	7	0 (0.11)	0 (3)
8	0 (45)	0 (30)	0 (0.01)	8	0 (0.11)	1.414 (6)
9	0 (45)	−1 (5)	−1 (0.02)	9	1.414 (0.2)	0 (3)
10	1 (65)	1 (60)	0 (0.01)	10	1 (0.15)	−1 (1.5)
11	0 (45)	0 (30)	0 (0.01)	11	0 (0.11)	0 (3)
12	−1 (RT)	0 (30)	1 (0.0067)	12	0 (0.11)	0 (3)
13	−1 (RT)	0 (30)	−1 (0.02)	13	0 (0.11)	−1.414 (0.5)
14	1 (65)	0 (30)	−1 (0.02)			
15	0 (45)	−1 (5)	1 (0.0067)			

ml^{-1}) at three coded levels (high (+1), middle (0), low (−1)) were examined to optimize these parameters' effects and interactions on the responses *i.e.* maximizing the removal efficiencies of the trace metals individually (single-objective) and collectively (multi-objective). For both optimizations, range and levels of each factor are provided in Table 1.

On contrary, for Optimization-2, RSM with CCD having two independent factors *i.e.* dose of PF (g) and biosorption time (h) at five coded levels (extreme maximum (+α = 1.414), and extreme minimum (−α = −1.414), high (+1), middle (0), low (−1)) were examined to study the parameters' interactions and their effects on the responses. CCD is a five-level fractional factorial design comprising a two-level factorial design, central points, and two axial points. Since it is based on a two-level factorial design, CCD is well-suited for a smaller number of independent variables. Hence, CCD was employed for Optimization-2 due to the limited number of input variables and the need to identify extreme responses.[9,32,33] Table 2 shows the total number of experiments for both optimizations in a fully random order to avoid biases. For Optimization-1 and Optimization-2, 15 and 13 numbers of experimental runs were performed, respectively. More experimental runs in Optimization-1 than Optimization-2 are due to high numbers of factors. For both optimizations, the co-relationships between output responses *i.e.* removal efficiencies of trace metals (dependent variables) and involved factors (independent variables) are defined by the second order multi-variable polynomial regression eqn (1) as also reported in our previous studies.[9,10,34,35]

$$y = \beta_0 + \sum_{i=1}^{N} \beta_i x_i + \sum_{i=1}^{N} \beta_{ii} x_i^2 + \sum_{i \neq 1}^{N} \beta_{ij} x_i x_j + \varepsilon \quad (1)$$

where, y is the percent removal efficiency (dependent variable), x_i, x_j denote the coded variables (independent), β_0, β_i, β_{ii}, and β_{ij} are the model intercept, the linear, quadratic (squared) and cross interaction coefficients, respectively. N and ε are the no. of independent factors and model error term, respectively. The coded and actual values are associated with each other by the following eqn (2):

$$\text{Coded value} = \text{actual value} - \frac{\text{mean}}{\frac{\text{range}}{2}} \quad (2)$$

The goodness of the models (regression) was determined based on R^2 (adj. R^2) and other performance indicators' values which include root mean squared error (RMSE), percent relative error (RE) and mean absolute error (MAE) *etc.* Their correlations are provided in ESI.† For the graphical analyses of the data, MINITAB (ver. 18) software was used where analysis of variance (ANOVA) was implemented to determine the statistical significance of all parameters used in both optimizations. The basic difference between single and multi-objective optimization is the involvement of objective functions (OFs). Multiobjective optimization is performed by optimizing one OF at a time, and then finding the set of operating conditions that are optimal of all the OFs.

2.5 Physicochemical characterization

The physicochemical composition of PF was assessed through proximate and ultimate analyses. The elemental (ultimate) analysis was conducted using a CHNS_O analyzer (Perki-nElmer, series II CHNS/O analyser 2400). The sample was placed in a moisture analyzer (Mettler Toledo, HE53, Halogen Moisture Analyzer) and kept at 105 °C. The weight was recorded until it stabilized at 105 °C, following the ASTM E1756 standard. Ash content was determined by comparing the dry weight of the sample before and after igniting it overnight at 575 ± 25 °C.[36] For volatile matter (VM), a sample of 12 ± 0.02 mg was heated at a rate of 10 °C min^{-1} from 25 °C to 550 °C under a nitrogen flow of 60 ml min^{-1}, and the temperature was maintained at 550 °C for 60 min.[37] Fixed Carbon (FC) was calculated by subtracting the sum of ash, MC, and VM from 100, ensuring all values were on the same moisture reference base. Data obtained from ultimate analysis were utilized to determine the higher heating value (HHV) of PF and OPT2-ads using Milne eqn (3):[38]

$$\begin{aligned} \text{HHV (MJ kg}^{-1}) = {}& 0.341\,(\%\,\text{C}) + 1.322\,(\%\,\text{H}) \\ & + 0.0686\,(\%\,\text{S}) - 0.12\,(\%\text{O} + \%\,\text{N}) \\ & - 0.0153\,(\%\,\text{ash}) \end{aligned} \quad (3)$$

2.6 Kinetic evaluation and reaction mechanism

For non-isothermal decomposition of solid-state reactions can be expressed in mathematical form as eqn (4):

$$\frac{d\alpha}{dt} = k(T) \cdot f(\alpha) \quad (4)$$

where, $\frac{d\alpha}{dt}$ is the conversion rate, T is the absolute temperature, k is the rate constant depending upon temperature, $f(\alpha)$ is the differential mechanism function and α is the extent of conversion which can be equated as eqn (5):

$$\alpha = \frac{m_o - m_t}{m_o - m_f} \quad (5)$$

where 'm' (mg) is the mass of sample, m_o, m_t, and m_f are initial, actual and final masses of the sample, respectively.

The activation energy from the Arrhenius equation is expressed by eqn (6):

$$k(T) = k_0 \times \exp\left(-\frac{E}{RT}\right) \quad (6)$$

where 'k_0' is the pre-exponential factor (s^{-1}), 'R' is the universal gas constant (J mol^{-1} K^{-1}), 'E' is the activation energy (J mol^{-1}), 'T' is the reaction temperature (K). Substituting eqn (6) in (4), gives eqn (7) as given below:

$$\frac{d\alpha}{dt} = A \cdot \exp\left(-\frac{E}{RT}\right) \cdot f(\alpha) \quad (7)$$

The heating rate β (K min^{-1}) can be expressed as $\beta = \frac{dT}{dt}$, then for non-isothermal TGA experimental eqn (7) is expressed as eqn (8):

$$\frac{d\alpha}{dT} = \frac{A}{\beta}\cdot\exp\left(-\frac{E}{RT}\right)\cdot f(\alpha) \qquad (8)$$

Integrated form of the eqn (8) is given as follows in eqn (9):

$$g(\alpha) = \int_0^\alpha \frac{d\alpha}{f(\alpha)} = \frac{A}{\beta}\cdot\int_{T_o}^T \exp\left(-\frac{E}{RT}\right)dT \qquad (9)$$

where, $g(\alpha)$ is an integral reaction mechanism function. The algebraic forms of the differential and integral mechanism functions are depicted in ESI† (Table S1).

A flowchart outlining the overall experimental approach including pretreatment, optimization, thermal study, and valorization is presented as Scheme S1 in the ESI.†

3 Results and discussion

3.1 Pretreatment of PF (Optimization-1)

3.1.1 BBD and non-linear model development.
Optimization-1, pretreatment of PF, for the removal of metal ions was performed using RSM integrated with BBD approach. To achieve this, three factors such as process temperature (A), process time (B) and PF : THF ratio (C) were used with a total number of experimental runs of 15 at various conditions were studied. Removal efficiencies for all six trace metals (three cations and three oxyanions) were obtained by doing biosorption experiments using modified PF of 0.1 g in 10 ml of MMSW for 24 h with pH of 7.5. Experimental data of each treatment are depicted in Table 2 and then experiments were performed based on them and finally obtained the removal efficiencies for each of the trace metals. These experimental removal efficiencies were used to formulate the six different quadratic regression models (eqn (10)–(15)) in coded format as given below:

$$\begin{aligned} M1(Cr^{6+})\ (\%) = {}& 81.014 + 0.949A - 1.259B + 0.203C \\ & - 0.726A \times A - 1.284B \times B \\ & - 0.178C \times C - 1.014A \times B - 1.393A \\ & \times C - 0.674B \times C \end{aligned} \qquad (10)$$

$$\begin{aligned} M1(As^{3+})\ (\%) = {}& 54.63 - 3.63A + 2.53B \\ & - 0.13C + 1.03A \times A + 2.31B \times B \\ & + 2.97C \times C - 0.92A \times B + 4.19A \\ & \times C + 3.74B \times C \end{aligned} \qquad (11)$$

$$\begin{aligned} M1(V^{5+})\ (\%) = {}& 73.66 - 5.90A + 1.34\,B \\ & - 2.04C - 7.09A \times A - 0.40B \times B \\ & - 12.85C \times C - 3.16A \times B + 0.76A \\ & \times C + 4.43B \times C \end{aligned} \qquad (12)$$

$$\begin{aligned} M1(Co^{2+})\ (\%) = {}& 52.73 + 0.150A + 0.273B \\ & + 0.629C - 0.89A \times A - 0.62B \times B \\ & - 0.46C \times C - 0.36A \times B + 0.81A \\ & \times C - 0.28B \times C \end{aligned} \qquad (13)$$

$$\begin{aligned} M1(Ni^{2+})\ (\%) = {}& 64.03 + 1.08A - 1.85B \\ & + 1.84C + 0.61A \times A - 2.79B \times B \\ & - 0.57C \times C - 1.65A \times B - 1.73A \\ & \times C - 0.51B \times C \end{aligned} \qquad (14)$$

$$\begin{aligned} M1(Cd^{2+})\ (\%) = {}& 96.491 - 0.158A - 0.054B \\ & - 0.329C - 0.325A \times A - 0.298B \\ & \times B - 0.861C \times C - 0.426A \times B \\ & + 0.250A \times C + 0.328B \times C \end{aligned} \qquad (15)$$

where, A, B, and C represent process temperature (°C), process time (min) and PF : THF ratio (g ml^{-1}), respectively. M1 represents the predicted percentage value for each response in Optimization 1. These models are presented in the form of coded variables for all statistical analyses to maintain experimental design as orthogonal as it helps in estimating model terms independently (*i.e.*, bias free) and hence making the analyses straightforward.[9,34]

Fig. 1 presents the regression plots comparing the model predictions to the experimental data (within ±10% tolerance) for each run. Respective errors for each test run were also calculated and they were reasonably small, indicating that experimental values are close enough to the predicted values (Table S2†). R^2 and adj R^2 values for all the trace metals were reasonable indicating that the experimental data fitted well with the regression models. R^2 values of Cr^{6+}, V^{5+}, As^{3+}, Ni^{2+}, Co^{2+} and Cd^{2+} were 84.2(83.0), 73.2(71.2), 67.2(64.6), 57.6(54.3), 23.5(17.6), and 73.3(71.5), respectively.

The range of R^2 values provided an indication that the predicted models had relatively high standard deviations. Hence, suggested further optimization at wider range of experimental data for more reliable and better prediction.[9,39] Regression models at higher polynomial order are also plotted and provided in ESI† (Fig. S1). The goodness of the models was further scrutinized by implementing RMSE and MAE indicators. The outcomes from these indicators were reasonably low (Table S3†) for all responses that provided us with confidence in the predictions of our models. However, the predicted outcomes (% removals) from the developed models were low for most of the trace metals. To find which interaction(s) and factor(s) are statistically significant on the responses in the predicted models, ANOVA analysis was used (Table 3a). The factor was assumed to be significant at the significant level of 10% ($p < 0.1$) based on literature.[9,39,40] It can be clearly seen that constants for all responses are significant. Other than constants, very few interactions of the factors are found to be significant. For instance, in case of Cr^{6+}, only linear interaction of pretreatment temperature ($p = 0.084$) and pretreatment time ($p = 0.036$) were found to be significant. Additionally, the square of pretreatment time ($p = 0.105$) and cross interaction of pretreatment temperature with ratio ($p = 0.076$) were significant. Other than them, none of the interactions were significant for Cr^{6+}. For the rest of the responses, none of the interactions were significant except product of ratio for the Cd^{2+} and V^{5+}. Table 3a also shows the relative errors among the coefficients of each factor on the responses which were also reasonably low.

3.2 Process parameters biosorption (Optimization-2)

3.2.1 CCD and non-linear model development.
Optimization-2, process parameters biosorption, was performed to improve the removal of trace metals from MMSW and
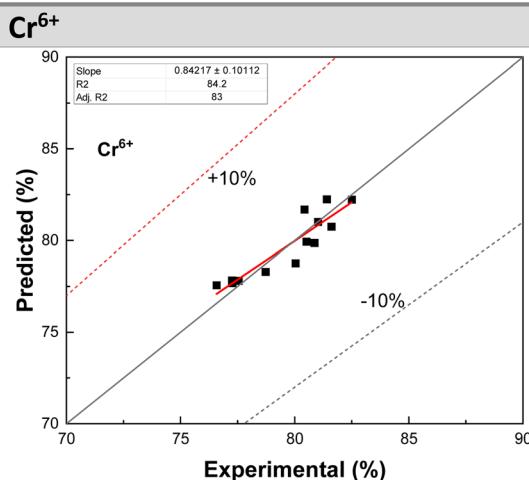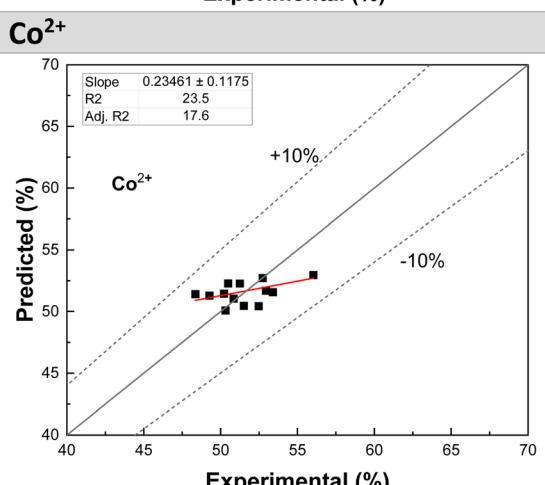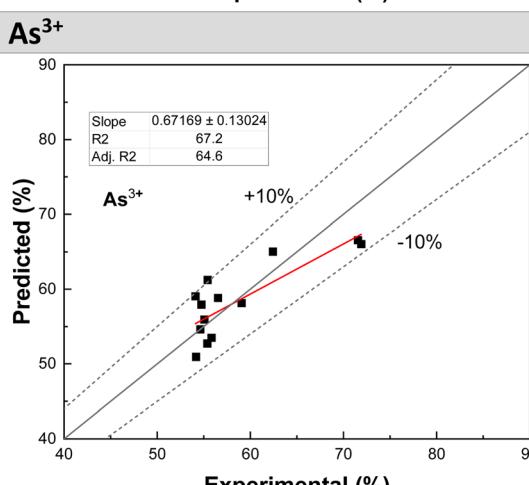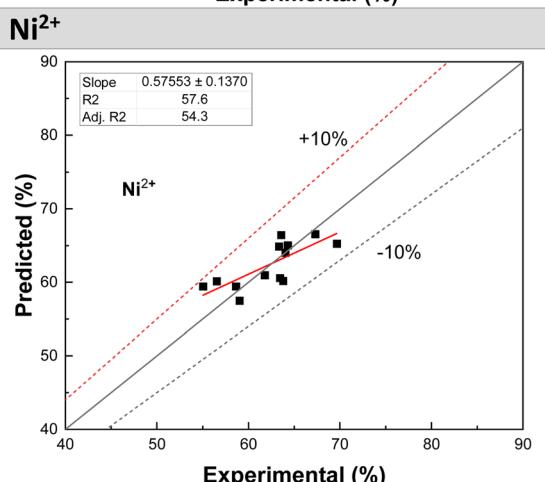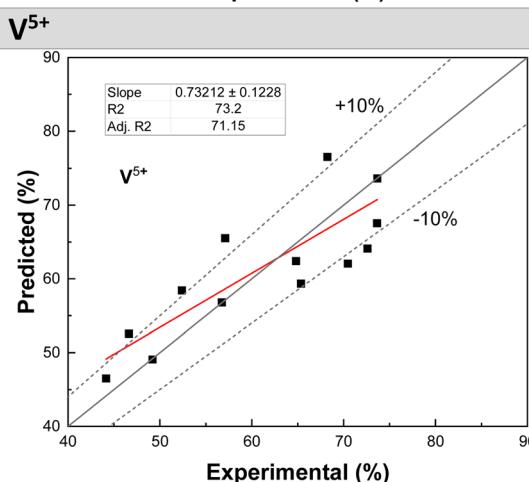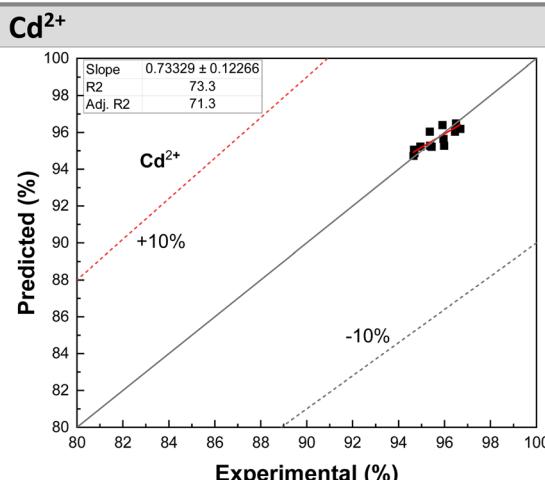
Fig. 1 Experimental data *vs.* model predictions with ± 10 tolerance for the removal efficiencies of three cations (Ni^{2+}, Co^{2+}, Cd^{2+}) and three oxyanios (V^{5+}, As^{3+}, Cr^{6+}) from MMSW (including all interactions and full factors) for Optimization-1.

for that purpose RSM integrated with CCD approach was used. To achieve this, two factors such as dose of PF and biosorption time were used with a total number of experimental runs of 13 at various conditions were studied.

Like Optimization-1, removal efficiencies for all six trace metals were obtained by doing biosorption experiments using different amounts of modified PF in MMSW (10 ml) at different biosorption times while keeping the pH at 7.5. It is vital to

Table 3 ANOVA analysis (p-values and standard errors of each coefficient) of all response surface second order regression models (a) Optimization-1 (b) Optimization-2

(a)

	Standard error (SE) coefficients						p-value					
	Oxyanions			Cations			Oxyanions			Cations		
Factor	Cr^{6+}	As^{3+}	V^{5+}	Co^{2+}	Ni^{2+}	Cd^{2+}	Cr^{6+}	As^{3+}	V^{5+}	Co^{2+}	Ni^{2+}	Cd^{2+}
Const.	0.720	3.31	5.41	1.61	2.42	0.370	0.000	0.000	0.000	0.000	0.000	0.000
A	0.441	2.03	3.31	0.984	1.48	0.227	0.084	0.133	0.135	0.885	0.501	0.518
B	0.441	2.03	3.31	0.984	1.48	0.227	0.036	0.267	0.702	0.792	0.267	0.822
C	0.441	2.03	3.31	0.984	1.48	0.227	0.665	0.951	0.564	0.551	0.271	0.206
A^2	0.649	2.99	4.88	1.45	2.18	0.334	0.314	0.743	0.205	0.567	0.791	0.374
B^2	0.649	2.99	4.88	1.45	2.18	0.334	0.105	0.474	0.938	0.688	0.258	0.413
C^2	0.649	2.99	4.88	1.45	2.18	0.334	0.795	0.365	0.046	0.764	0.804	0.049
$A \times B$	0.623	2.87	4.68	1.39	2.10	0.321	0.165	0.761	0.530	0.808	0.467	0.242
$A \times C$	0.623	2.87	4.68	1.39	2.10	0.321	0.076	0.204	0.878	0.587	0.449	0.471
$B \times C$	0.623	2.87	4.68	1.39	2.10	0.321	0.329	0.249	0.388	0.848	0.816	0.353

(b)

	Standard error (SE) coefficients						p-value					
	Oxyanions			Cations			Oxyanions			Cations		
Factor	As^{3+}	V^{5+}	Cr^{6+}	Co^{2+}	Ni^{2+}	Cd^{2+}	As^{3+}	V^{5+}	Cr^{6+}	Co^{2+}	Ni^{2+}	Cd^{2+}
Const.	0.410	0.330	0.449	0.578	0.447	0.212	0.000	0.003	0.000	0.000	0.000	0.000
X	0324	0.261	0.355	0.457	0.353	0.167	0.000	0.000	0.958	0.985	0.000	0.003
Y	0.324	0.261	0.355	0.457	0.353	0.167	0.000	0.094	0.445	0.014	0.000	0.984
X^2	0.348	0.280	0.381	0.490	0.379	0.180	0.025	0.105	0.041	0.002	0.697	0.000
Y^2	0.348	0.280	0.381	0.490	0.379	0.180	0.487	0.162	0.471	0.739	0.042	0.553
$X \times Y$	0.459	0.369	0.502	0.647	0.500	0.237	0.016	0.590	0.306	0.098	0.013	0.728

mention here that the modified PF used in Optimization-2 was prepared at the optimized set of conditions of Optimization-1 to maximize the removal of trace metals from MMSW. Experiments were then performed and finally obtained the removal efficiencies for each of the trace metals. These experimental removal efficiencies were used to formulate the six different quadratic regression models (eqn (16)–(21)) in coded format as given below:

$$M2\ (V^{5+})\ (\%) = 79.567 + 1.824X + 0.505Y \\ - 0.522X \times X + 0.437Y \times Y \\ + 0.208X \times Y \tag{16}$$

$$M2\ (Cr^{6+})\ (\%) = 56.311 + 0.020X + 0.287Y \\ - 0.953X \times X - 0.290Y \\ \times Y - 0.554X \times Y \tag{17}$$

$$M2\ (As^{3+})\ (\%) = 58.862 + 6.995X + 3.366Y \\ + 0.993X \times X + 0.255Y \\ \times Y + 1.456X \times Y \tag{18}$$

$$M2\ (Co^{2+})\ (\%) = 81.060 - 0.009X - 1.484Y \\ - 2.292X \times X + 0.170Y \times Y \\ - 1.235X \times Y \tag{19}$$

$$M2\ (Ni^{2+})\ (\%) = 78.224 - 2.879X - 2.208Y \\ + 0.154X \times X + 0.942Y \\ \times Y - 1.662X \times Y \tag{20}$$

$$M2\ (Cd^{2+})\ (\%) = 96.556 + 0.728X - 0.004Y \\ - 1.097X \times X + 0.112Y \\ \times Y - 0.086X \times Y \tag{21}$$

where, X, and Y represent dose of modified PF (g) and biosorption time (h), respectively. M2 represents the predicted percentage value for each response in Optimization 2. These models are again presented in the form of coded variables for all statistical analyses.

Fig. 2 shows the regression plots comparing the model predictions to the experimental data (within ±10% tolerance) with respect to each run for all trace metals. Respective errors for each test run were also reasonably small, indicating that experimental values are close enough to the predicted values (Table S4†). R^2 and adj R^2 values for all the trace metals were reasonable. R^2 values of V^{5+}, As^{3+}, Cr^{6+}, Ni^{2+}, Co^{2+} and Cd^{2+} were found to be 89.5 (88.5), 98.8 (98.7), 54.4 (50.2), 94.6 (94.1), 84.1(82.6), and 89.3(88.3), respectively. The range of R^2 values provided an indication that the predicted models had relatively low values of standard deviations compared to Optimization-1. However, models still could not explain 1–10% of the

experimental results. Like Optimization-1, the outcomes of RMSE and MAE of Optimization-2 were also low for all responses (Table S3†). Furthermore, the predicted removals (%) from the developed models of almost all trace metals were improved, *i.e.* removal efficiencies were relatively higher for most of the metals compared to Optimization-1 values.

It is widely accepted that the responses behave differently by the effect of different levels of the factors and due to the complex nature of the bio-sorbent used. From Fig. 3a of the main effect plots, both factors showed great magnitude of the slope, hence showed great main effects on the responses. However, their results seemed to be controversial. In case of
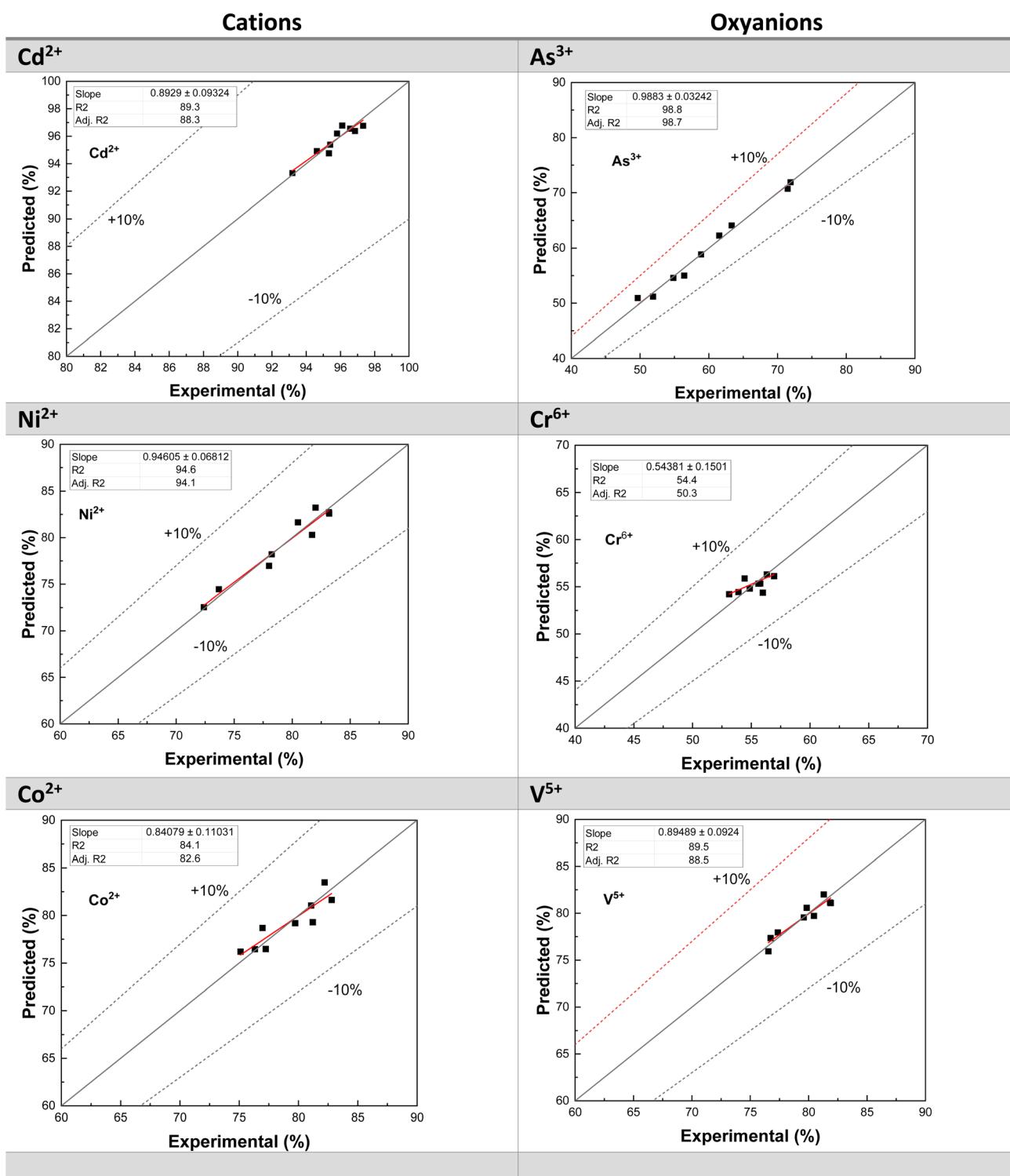

Fig. 2 Experimental data *vs.* model predictions with ±10 tolerance for the removal efficiencies of three cations (Ni^{2+}, Co^{2+}, Cd^{2+}) and three oxyanios (V^{5+}, As^{3+}, Cr^{6+}) from MMSW (including all interactions and full factors) for Optimization-2.

biosorbent dose, sorption of most of the oxyanions (V^{5+} and As^{3+}) increased linearly with the increase of biosorbent dose. This increase is attributed to the availability of the more vacant sites (exchangeable) for the sorption and increase in surface with the increase of dose of the biosorbent. On the other hand, cations (Co^{2+} and Cd^{2+}) sorption first increased and then decreased with the increase of PF dose. Additionally, the sorption of Ni^{2+} decreased linearly with the increase of PF dose. This clearly indicates the dominant nature of oxyanions over the cations may be due to their high values of surface charge and low ionic radii.[41] These oxyanions kept on occupying the available sites as a result less sites were available for the sorption of cations hence decreased with the increase of sorbent dose. Additionally, the sorption process of trace metals is highly dependent on competition with each other and their complexation with active sites present in PF. These interactions of trace metals with PF can be explained from their Lewis acid and base principles.[31] In case of time, most of the cations and oxyanions showed the increasing trend of the sorption process at higher adsorption time. As the time increased, the sorbate got enough time to disperse and adsorbed on to the surface and inside the pores. Hence upon increasing the sorption time, the adsorption also increased which also agreed with the findings in literature.[42–45] It seems from main effect plots that both factors are affecting the biosorption of trace metals. However, the biosorbent's dose is found to be more significant than biosorption time as shown by the Pareto charts (provided in ESI† as Fig. S2). On the other hand, an interaction plot is a visual representation of the interaction between the effects of two factors. From Fig. 3b, it can be clearly seen that both factors showed great interactions on all the responses of trace metals. However, there was no interaction of these factors on As^{3+} observed. This could be the reason for the rapid uptake of As^{3+} by the PF. It was also observed that most of the interactions took place at low to high levels of the factors. Main effect plots and interaction plots for Optimization-1 were also generated and provided in ESI† as Fig. S3 and S4.

In Optimization-2, based on ANOVA analysis, the constants of all models for all responses are significant like Optimization-1 (Table 3b). Other than constants, some of the interactions of the factors are significant. For instance, in case of As^{3+} (oxyanions), linear interaction of both X ($p = 0.000$) and Y ($p = 0.000$), product interaction of X ($p = 0.025$) and cross interaction of X and Y ($p = 0.016$) were significant. Other than them, none of the interactions were significant for As^{3+}. Additionally, it can be seen clearly that the interaction of X is involved in all responses. Whereas Y interactions are also significant for most of the responses except for Cd^{2+} and Cr^{6+} where they are insignificant, indicating that X is the most dominant factor between X and Y which is also consistent with main effect findings. For the rest of the responses, p-values of X and Y factors show the relative error among the coefficients of each factor on the responses which are also reasonably low. To assess whether these data values are normally distributed or not, different residual plots (histogram, residual, normal probability etc.) were generated. Bell shape of data points in histograms, linear patterns of points on residual and normal probability plots indicated that
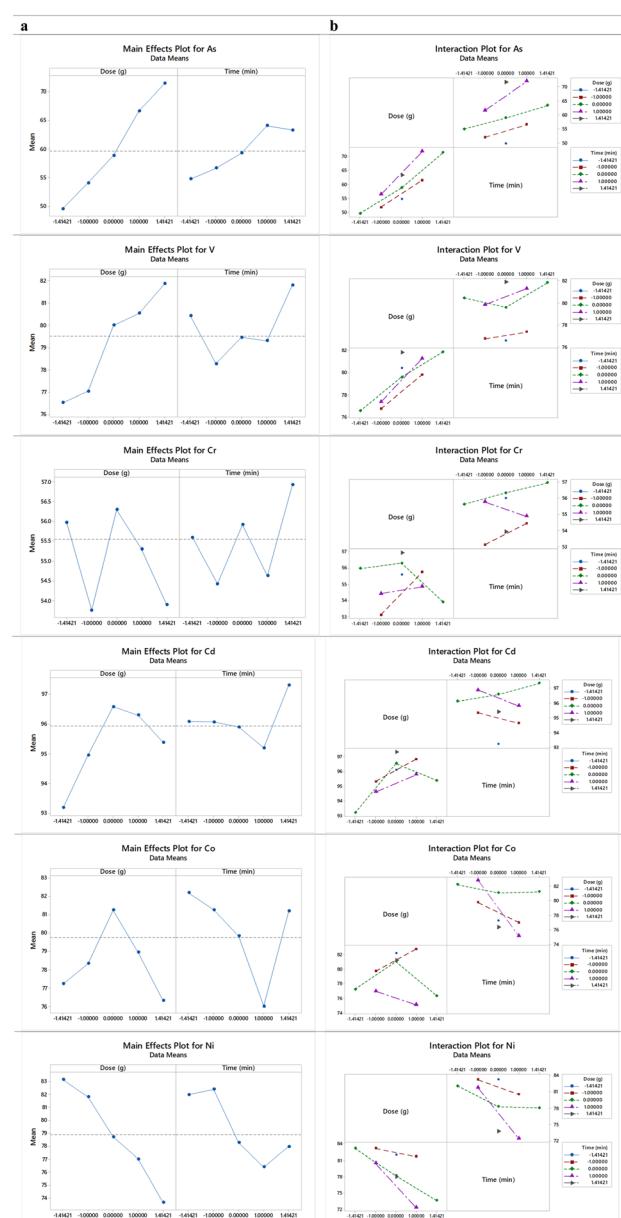

Fig. 3 (a) Main effect plots and (b) interaction plots of independent parameters (e.g., dose of PF and bio-sorption time) on the removal of three oxyanios (V^{5+}, As^{3+}, Cr^{6+}) and three cations (Ni^{2+}, Co^{2+}, Cd^{2+}) from MMSW (Optimization-2) [above three: oxyanions; below three: cations].

data is normally distributed and good for the model data sets (figures are provided in ESI† for both optimizations as Fig. S5).

3.3 Single and multi-objective optimizations

3.3.1 Single-objective optimization. Initially, single optimizations of the six different metals i.e. three oxyanions (As^{3+}, V^{5+}, Cr^{6+}) and three cations (Cd^{2+}, Co^{2+}, Ni^{2+}) were performed separately. To visualize the interaction effects on them, 2D contour and 3D response surface plots were generated and provided in ESI† as Fig. S6 (Optimization-1) and Fig. S7 (Optimization-2). A topographical behavior of contour plots and
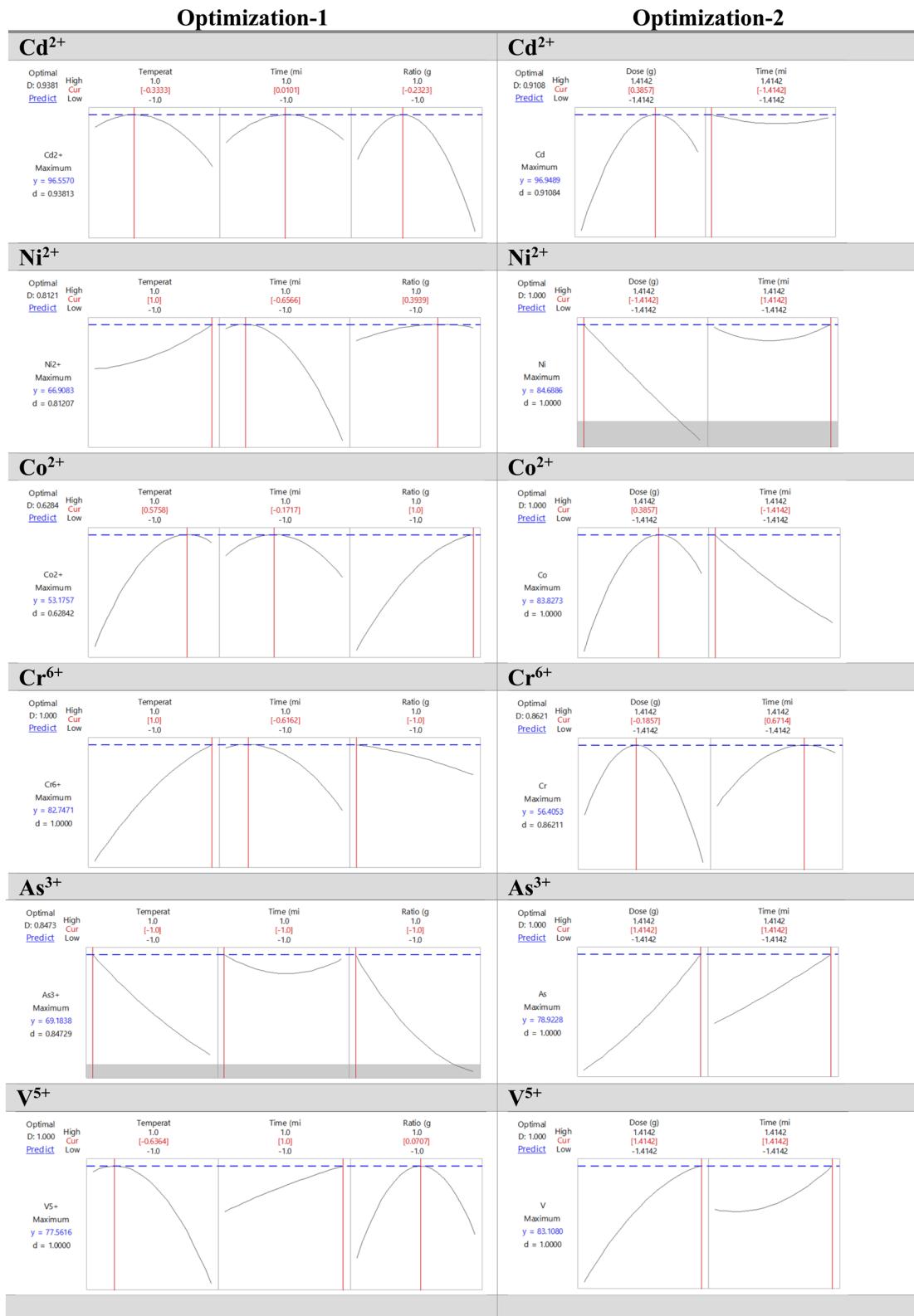
Fig. 4 Response optimizer plots for the single-objective optimization of Optimization-1 and Optimization-2. Here, D and d are overall and individual desirability functions of the response, respectively (ideal value of d or $D = 1$). Lo, Cur, and Hi are low, current and high factor levels in coded values, respectively.

concave feature of surface plots were observed. From their curvatures, the optimum operating condition can be spotted either at the center of contour plot or at the top of the surface plots. However, the exact value of a single optimal set of operating conditions is difficult to find from them. For that purpose, individual response optimizer plots for all six metals were generated, as given in Fig. 4a and b. In optimizer plots, columns show the influence of each factor (columns) on all responses and rows present the desirability functions (d or D). The red vertical lines on the optimizer plot show the optimal setting of the factors. The optimum coded values (in red) of the current factor level are presented at the top of the columns. For instance, optimum coded values of temperature, time and ratio are −0.3333, 0.0101, and −0.2323, respectively. These coded values lead to actual values for temperature (38 °C), time (33 min) and ratio (0.011) which results in the highest possible removal of Cd^{2+} *i.e.* 96.55%. Similarly, the maximum V^{5+} removal of 77% was obtained at optimal set of parameters (32 °C, 60 min and 0.014 ratio). Rest of metal removals (%) and their optimal set of conditions are presented in Table 4.

In engineering research, the desirability function (d or D) approach has been extensively utilized for optimization, considering the maximum performance.[46,47] Individual desirability function values are close to ideal value for most of the trace metals (Table 4). Single optimizer plots showed the highest possible removals but at different optimal set of conditions for each trace metal. Hence, there is a need to obtain the best optimal set of conditions for all responses at their maximum possible removals. For that purpose, multi-objective optimization was used which is an interesting and hot topic in literature involving the conflicting objectives to be solved simultaneously.[39,48,49]

3.3.2 Multi-objective optimization. For multi-objective optimization, it is vital to compare the trade-offs of each objective and then choose the best conditions to maximize multiple responses/objectives simultaneously.[39,49] To obtain a single optimal solution in multi-objective optimization of MMSW, overlaid contour plots of three possible combinations for all six responses (Cd^{2+}, Co^{2+}, Ni^{2+}, Cr^{6+}, V^{5+}, and As^{3+}) were plotted to find the distinctive operating conditions of the sorption process. Fig. 5a and b shows one possible combination of overlaid contour plots for each optimization, with other combinations available in the ESI† as Fig. S8. The solid lines in the overlaid contour plots indicate the highest values of the responses and the dotted lines show the lowest values of all responses. The optimum operating values of the independent variables are indicated by the white region in the overlaid contour plots. From the plots (white region), it is observed that all responses *viz.*, are maximized simultaneously by trading off the maximum removal efficiencies of trace metals and optimizing the values of parameters. For Optimization-1, pretreatment temperature which is close to low level (−1) and ratio which is in between center level (0) to high level at holding pretreatment time at center level (0) (Fig. 5a). On the other

Table 4 Percent removal of metals and their optimal set of conditions for both optimizations along with their desirability function values (single and multi-objective)

First optimization (pre-treatment of PFs)

| Metals | Single-objective optimization | | | | | Multi-objective optimization | | | | |
	T (°C)	t (min)	Ratio (−)	Removal (%)	Desirability function (d)	T (°C)	t (min)	Ratio (−)	Removal (%)	Desirability function (d)
Cd^{2+}	38	33	0.011	96.56	0.938	30	47	0.015	96.27	0.800
Ni^{2+}	65	14	0.015	66.91	0.812				63.38	0.571
Co^{2+}	56	28	0.02	53.17	0.628				52.16	0.496
V^{5+}	32	60	0.014	77.56	1.000				74.40	1.000
As^{3+}	25	5.0	0.0067	69.18	0.847				60.03	0.333
Cr^{6+}	65	16	0.0067	82.74	1.000				79.59	0.508
										$D = 0.581$

Second optimization (process parameters)

| Metals | Single-objective optimization | | | | Multi-objective optimization | | | |
	t (h)	Dose (g)	Removal (%)	Desirability function (d)	Dose (g)	t (h)	Removal (%)	Desirability function (d)
Cd^{2+}	0.5	0.14	96.94	0.911	0.17	0.5	96.87	0.893
Ni^{2+}	6.0	0.02	84.69	1.000			82.95	0.979
Co^{2+}	0.5	0.14	83.82	1.000			83.66	1.000
V^{5+}	6.0	0.20	83.11	1.000			84.49	0.740
As^{3+}	6.0	0.20	78.92	1.000			58.20	0.385
Cr^{6+}	4.8	0.09	56.40	0.862			55.44	0.611
								$D = 0.731$

hand, for Optimization-2, dose of PF is at 1.414 and biosorption time is at −1.414 levels (Fig. 5b).

The accuracy and optimum conditions are not completely identified from the overlaid contour plots; thus, multi-objective optimizer plots were generated that combined the maximum percent removals of all trace metals at optimal set of conditions of the factors, as shown in Fig. 5c and d. For Optimization-1, the optimal set of coded values for pretreatment temperature, pretreatment time and PF : THF ratio, are −0.7374, 0.5152, and 0.3333, which are equivalent to actual values of 30 °C, 47 min and 0.015 g ml^{-1}, respectively. Similarly, for Optimization-2, the optimal set of coded values for dose and time are 0.6435, and −1.4142, which are equivalent to actual values of 0.17 g, and

30 min, respectively. Due to this two-step optimization approach at the optimal set of conditions, the predictions of percentage removals of all metals either remained about the same (Cd^{2+}, As^{3+}) or increased (Co^{2+}, Ni^{2+}, V^{5+}) compared to first optimization except Cr^{6+} suggesting that the optimal conditions and the specific pH were not favorable for removal of the Cr^{6+} ions. *i.e.* its adsorption decreases significantly with the increase of pH due to negative surface charge on the surface as discussed in literature.[50,51] The percentage removal increased (+)/decreased (−) of the trace metals are +31.5%, +19.52%, +0.6%, −24.15%, −1.83%, and +6.09% for the Co^{2+}, Ni^{2+}, Cd^{2+}, Cr^{6+}, As^{3+}, and V^{5+}, respectively at the obtained optimal set of conditions after trading off. In fact, biosorption using PF is
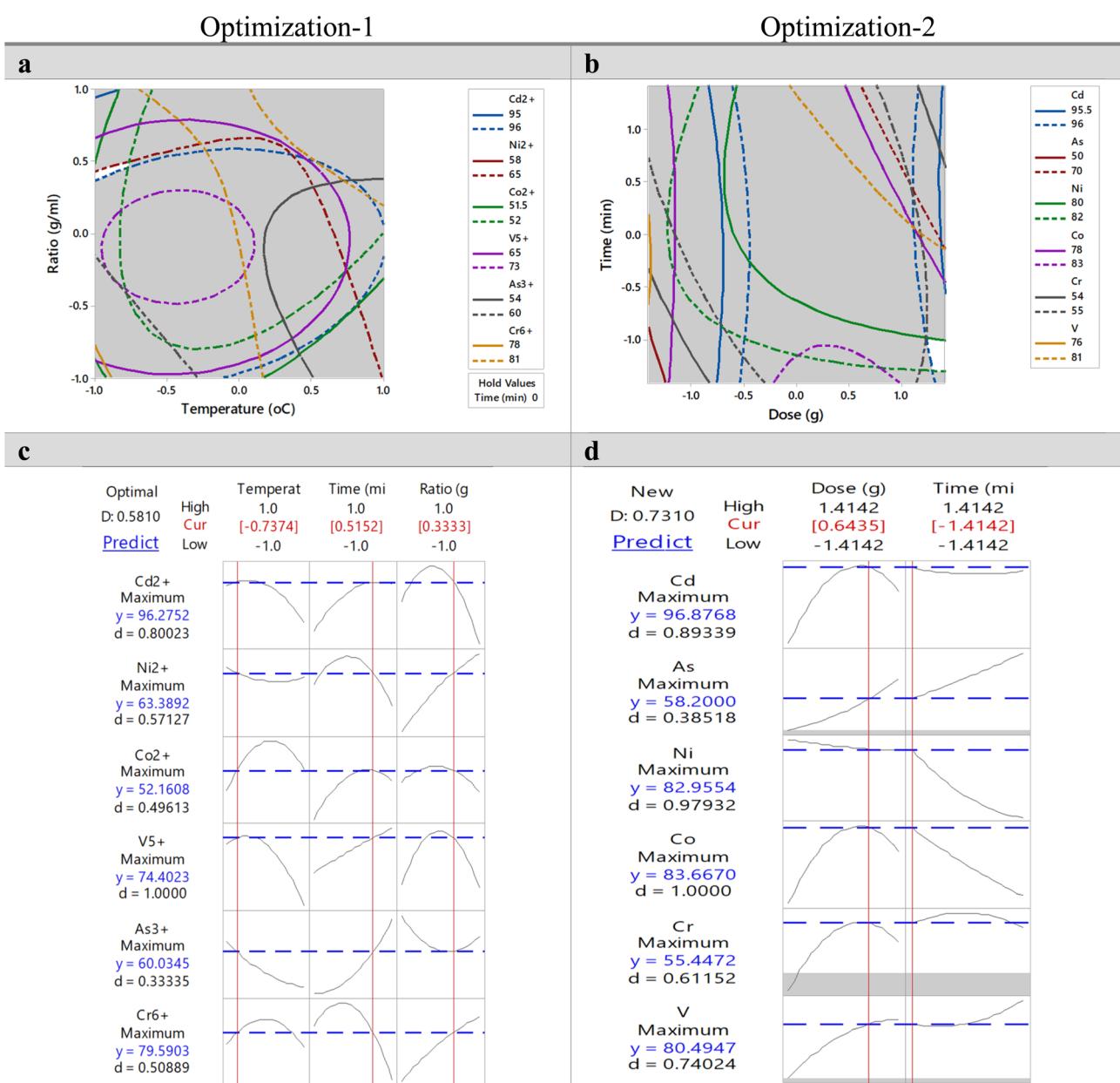

Fig. 5 Set of optimal conditions for the removal of oxyanions and cations in multi-objective optimization (a) overlaid contour plot for Optimization-1 (b) overlaid contour plot for Optimization-2 (c) optimizer plot for Optimization-1 and (d) optimizer plot for Optimization-2.

a complicated process and hence involves several other factors and parameters such as pH of the solution, electronegativities, covalent indices, hydration energies of the trace metals for their removals. In addition to these influencing factors, several mechanisms such as complexation, ion exchange, coordination, and chelation, contribute to the removal of trace metals by bio-sorbents.[43] The underlying adsorption processes can be more clearly understood by examining the surface functional groups of biopolymers, which are crucial for metal ion binding and removal from wastewater. Since PFs are rich in keratin, their molecular structure contains a variety of nitrogen- and oxygen-containing functional groups. The nitrogen-based groups include both protonated species (NH_3^+, $C=N$, $C–NH$, $C–NH–C/C=NH_2^+$) and unprotonated amines (NH_2), while the oxygen-based groups comprise hydroxyl ($C–OH$), carbonyl ($C=O$), and carboxylate ($O=C–O^-$) moieties.[31] Analytically and mechanistically, the removal of these metals (oxyanions and cations) by biosorption process using PF has been discussed in detail in our previous studies.[3,31] Due to dual optimization, the composite desirability value in the second optimization ($D = 0.731$) was also found to be increased compared to first one ($D = 0.581$) (Table 4). Reasonably high value of D indicated that the optimal combination of variables identified in this study was favorable for simultaneously maximizing all responses. Additionally, the D value found in this study is reasonably high compared to the literature value[52,53] which give strength and confidence to our predicted results *i.e.* predictions are remarkably considered as realistic.

To confirm the optimal conditions for the biosorption of oxyanions and cations, a series of triplicate experiments were conducted at the optimum conditions of both optimizations, and the mean values for each metal ion were reported in Table 5. In Optimization-1, varying dosages (0.1, 0.15, and 0.2 g) of the pretreated PF were used for each metal ion using the OFAT approach while keeping time and pH constant. For each metal ion, the percentage errors were calculated and found to be reasonable, though slightly high for V^{5+} and As^{3+}, but these errors decreased as the dosage increased. The reasonable percentage error values indicate a good agreement between experimental results and model predictions, suggesting that the model can adequately describe the maximum removal of all metal ions from MMSW in Optimization-1. In Optimization-2, the model predictions closely matched the experimental data, especially for the cations, which had fewer errors. However, the models did not fit well with the oxyanions, indicating that the number of parameters selected in Optimization-2 were insufficient, as the biosorption process is influenced by multiple factors. Overall, the current study shares a simple pivotal platform that could facilitate the scale-up of PFs as waste material for the advanced research in the field of renewable energy, wastewater treatment *etc.*

3.4 Thermal behavior and reactivity analysis

3.4.1 Physicochemical characterization. The ultimate and proximate analyses of parent PF and OPT2-ads along with other notable biomasses like garlic husk, CFs, and banana leaves are

Table 5 Validation of the predicted metal ions removals at the optimal sets with the corresponding experimental data

		V^{5+}	Cr^{6+}	Co^{2+}	Ni^{2+}	As^{3+}	Cd^{2+}
Optimization 1							
Model predictions		74.40	79.59	52.16	63.38	60.03	96.27
Experimental values	0.10 g	44.69	82.31	51.56	69.15	48.86	92.45
	0.15 g	69.97	81.60	54.61	65.49	55.32	94.75
	0.20 g	81.17	79.38	55.86	58.79	58.73	94.07
% Errors	0.10 g	39.93	3.42	1.16	9.10	18.61	3.97
	0.15 g	5.95	2.53	4.75	3.33	7.85	1.58
	0.20 g	9.10	0.26	7.18	7.24	2.17	2.29
Optimization 2							
Model predictions		80.49	55.44	83.66	82.95	58.2	96.87
Experimental values	0.17 g	49.38	40.14	82.73	85.65	11.42	96.07
% Errors		38.65	27.60	1.11	3.25	80.38	0.83

compared in the provided Table 6. Biomasses with less than 10% moisture content are ideal for pyrolysis applications, including gasification, combustion, and conversion processes.[54] The proximate analysis shows that PF has a moisture content of approximately 8.5 wt%, which is below the acceptable threshold. This low moisture content allows for safe long-term storage with no concerns of deterioration due to microbial growth. With 8% moisture content, PFs can absorb enough water to prevent static buildup, beneficial in applications sensitive to static electricity.[36] The parent PF sample has a VM content of 64.56 wt%, FC content of 26.56 wt%, and very low ash content of 0.38 wt%, making it a suitable fuel. High VM content and low ash content make ignition easier, while high ash content increases processing costs, reduces energy conversion efficiency, slows the combustion process, and creates disposal issues.[55] The low moisture and ash contents of PF make it suitable for fuel and energy production, as both factors can negatively impact combustion.[56] PF also has a high FC content, contributing to heat generation during combustion due to its high energy value. The ultimate analysis indicates that PF contains high levels of carbon (48.16 wt%) and hydrogen (7.37 wt%), making it a viable feedstock for fuel and energy production. However, PF has higher sulfur (2.11 wt%) and nitrogen (14.85 wt%) contents compared to other biomasses like banana leaves and mustard stalk, but slightly lower than CFs. Low sulfur content indicates the presence of cysteine protein and suggests low SOx emissions. High nitrogen content implies PF can be used for producing bio-compost or animal feed. The bioenergy potential of PF is confirmed by its HHV, which is estimated to be 21.26 MJ kg^{-1}. This value is relatively high and comparable with other biomasses, including banana leaves (17.80 MJ kg^{-1}),[57a] rice husk (14.53 MJ kg^{-1}),[54] and pinewood (20.45 MJ kg^{-1}).[58]

CHNS_O analysis of the OPT2-ads sample was also conducted. The results showed a slight decrease in the C, H, and N contents, while the O and S contents increased slightly. The decrease in C and H can be attributed to the treatment of the PF sample with THF, which may have eroded the sample. Although the N content was still higher than in other biomasses, it was

Table 6 Ultimate and proximate analyses of the parent PF and OPT2-ads samples along with other biomasses from literature

Sample	Proximate analysis (wt%)				Ultimate analysis (wt%)					HHV (MJ kg^{-1})	Ref.
	M	VM	FC[a]	Ash	C	H	N	S	O[b]		
PF	8.50 ± 0.06	64.56	26.56	0.38 ± 0.02	48.16 ± 0.12	7.37 ± 0.04	14.85 ± 0.03	2.11 ± 0.0	27.13 ± 0.14	21.26	This study
OPT2-ads	11.8 ± 0.3	63.34	24.36	0.50 ± 0.10	46.41 ± 0.12	6.87 ± 0.55	14.42 ± 0.61	2.54 ± 0.13	29.28 ± 1.18	19.83	This study
Banana leaves	8.40	73.0	11.30	7.26	43.30	6.80	1.30	0.30	48.30	17.80	Singh et al.[57a]
Chicken feather	8.8–12.0	78–82	17–21	Very low	47.40	7.20	15.10	2.90	27.40	—	Tesfaye et al.[36]
Garlic husk	6.80	71.50	11.40	10.30	42.10	4.60	0.30	0.10	52.80	14.01	Singh et al.[57b]
Mustard stalk	8.96	70.80	12.90	7.36	43.70	5.80	0.60	0.30	46.20	16.94	Patidar et al.[25]

[a] Fixed carbon (% FC) = 100 − moisture (% M) − volatile matter (% VM) − % ash. [b] Oxygen (% O) = 100 − carbon (% C) − hydrogen (% H) − nitrogen (% N) − sulfur (% S) − % ash.

slightly less than in CFs. It is accepted that N-enriched samples typically exhibit lower surface electron density and greater π-electron accepting ability compared to N-free counterparts, owing to the high electronegativity of nitrogen atoms. Furthermore, the increased O/C (0.63) and (N + O)/C (0.942) atomic ratios in OPT2-ads indicate enhanced hydrophilicity and polarity of the material than parent PF sample. The increase in S content was likely due to the use of the metal stock solution. The H : C atomic ratio of the adsorbed sample (0.148) was lower than that of parent PF (0.153), indicating that OPT2-ads sample had higher aromaticity.[59] The ash content in OPT2-ads (0.5 wt%) was higher than in the parent PF (0.38 wt%) because of metal adsorption during the biosorption process. Despite this increase, the ash content in both samples is still low (less than 1.5 wt%), also making them suitable materials, along with the high VM content, for fixed bed gasification.[60] Moreover, the moisture content of the OPT2-ads sample increased, likely due to metal hydration following the adsorption process. The HHV (19.83 MJ kg^{-1}) of the OPT2-ads remained nearly unchanged compared to that of the parent PF. Overall, the abundance and physicochemical characteristics of parent PF and OPT2-ads samples make them suitable waste feedstocks for bioenergy production through thermal conversion processes.

3.4.2 **Thermal decomposition behavior.** To determine the thermal decomposition behavior of the parent PF and OPT2-ads samples, a simple thermal gravimetric (TG) analytic technique was used. Fig. 6 presents the TG and DTG profiles of OPT2-ads at different-heating rates (5,10, 20, 30 °C min^{-1}) for the pyrolyzed temperature from 25 to 700 °C for both OPT2-ads and parent PF. TG analyses were performed two times for each heating rate and their mean values were used for calculation. Parent PF was used for comparative study to see the effect of treatment on PF and understand the biosorption process in better way. Onsets, endsets, maximum temperature (Tm) and mass losses obtained from TG profiles at different heating rates are presented in Table 7. Onset temperature is the temperature at which significant weight loss begins, marking the initiation of the thermal decomposition process. Endset temperature, on the other hand, represents the point at which the major weight loss is complete, indicating the end of the decomposition phase. Both temperatures are usually determined by extrapolating tangents from the curve to pinpoint where the weight loss noticeably starts and ends. These temperatures were obtained using the method outlined in our previous studies.[61,62] Tm was determined from DTG peak at the respective heating rate.

It is observed that the patterns of mass losses at different heating rates look similar for both OPT2-ads and parent PF samples. However, their onsets, endsets, Tm, and percent mass losses were marginally different indicating that OPT2-ads sample is slightly more thermally stable than parent PF. For instance, in the case of OPT2-ads sample at 5 °C min^{-1}, its degradation behavior can be described into three main phases. Phase I is mass loss due to moisture loss (10.18%) in the temperature range of 25–262.79 °C. These moisture contents could be of three different types which exist inside the PFs i.e. loosely bound water, free water, and chemically bonded water
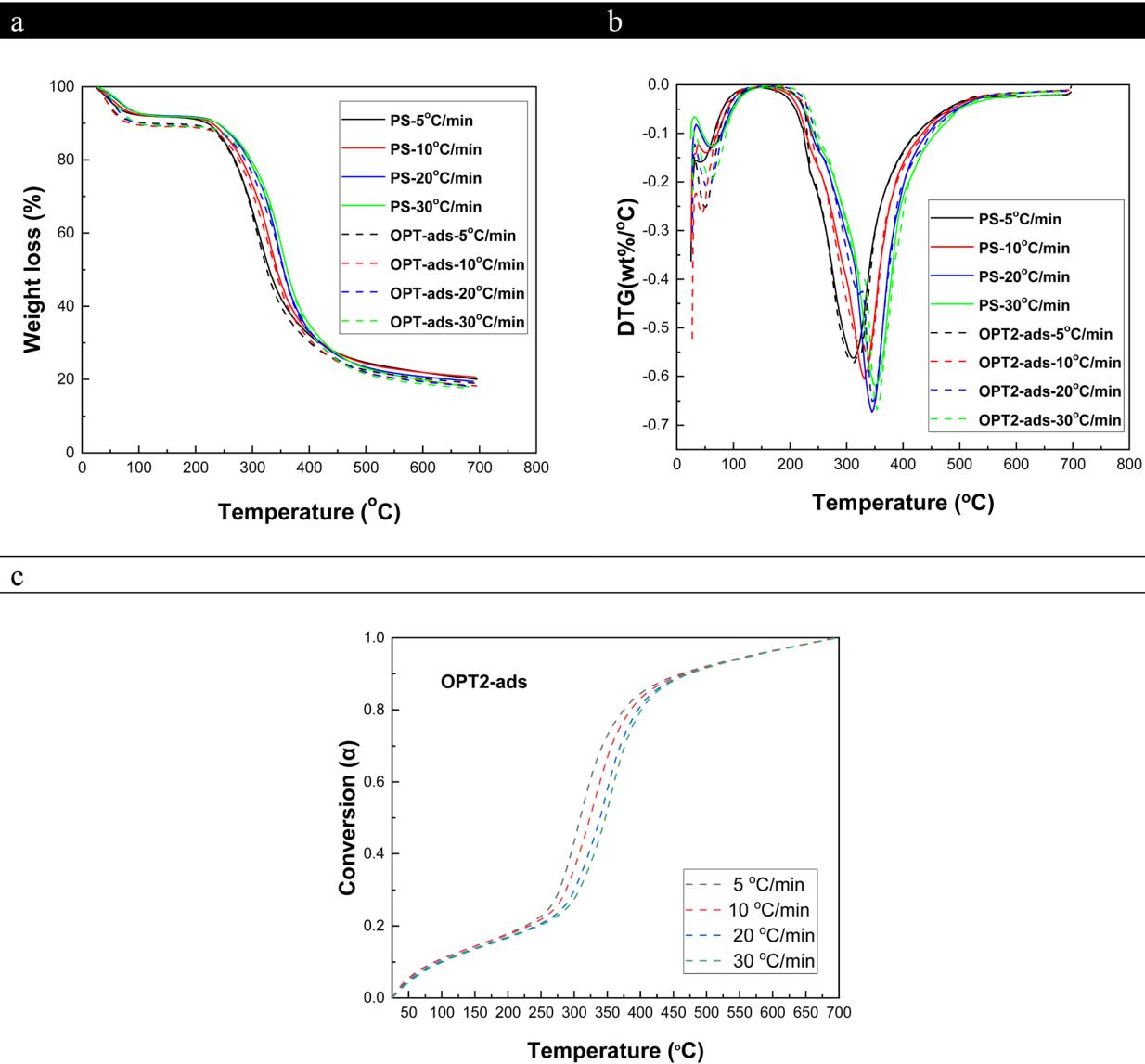
Fig. 6 (a) TGA profiles of OPT2-ads and parent PF (b) DTG profiles of OPT2-ads and parent PF (c) conversion *vs.* temperature of OPT2-ads sample at different heating rates.

which play a part in the conformational stability of keratin protein. The MC in OPT2-ads was slightly more than parent PF (8.25%) sample, due to the use of hydrated metal salt samples in the biosorption process. Phase II occurs in the temperature range from 262.79 °C to 373.25 °C due to the thermal denaturing of protein chain linkages and peptide bridge with the

Table 7 Onset, endset, Tm and mass loss% for parent PF and OPT2-ads samples at different heating rates

Heating rate (°C min⁻¹)	Parent PF						OPT2-ads					
	Onset (°C)	Endset (°C)	Tm (°C)	Mass loss (%)			Onset (°C)	Endset (°C)	Tm (°C)	Mass loss (%)		
				I	II	III				I	II	III
5	247.49	373.16	312.2	8.25	64.97	5.47	262.79	373.25	313.4	10.18	66.63	4.33
10	259.89	385.56	331.4	8.36	67.00	3.85	265.31	391.77	339.6	10.88	66.41	4.33
20	289.44	397.97	344.7	8.14	68.33	4.11	275.39	404.17	345.3	10.66	67.03	3.96
30	290.91	407.27	351.3	8.26	67.49	5.14	283.24	408.87	354.0	10.65	68.08	3.82

mass losses of *c.a.* 66.63%. This partial decomposition of the PFs is a complicated process which includes skeleton degradation and decomposition of protein units, depolymerization of peptide bridges, dehydration of the protein structure and thermal pyrolysis of peptide chain linkages. Additionally, this phase also involves removal of H_2S originating from the amino acid cysteine in keratin, denaturing of the predominantly beta-sheet structure, oxidation of carbon, destruction of H bonds, disulphide bonds between spiral peptide chain of the PF structure *etc.* Phase III occurs in the range of 373.16–700 °C which is due to the fully decomposition of PF with a mass loss of 4.33%. In this phase, PFs completely degrade to its elements which involve skeleton degradation and several reactions due to which keratins are degraded into lighter and volatile compounds like H_2O, CO_2, HCN and H_2S *etc.*[63] At around 550 °C, the mass loss appeared to stabilize, resulting weight losses of 4.33%, 4.33%, 3.96%, and 3.82% relative to the initial weights for heating rates of 5, 10, 20, and 30 °C min^{-1}, respectively. Beyond 550 °C, OPT2-ads samples were almost fully degraded, leaving carbonized residues accounting for 28.54%, 28.76%, 28.51% and 27.60% of the original OPT2-ads mass samples for heating rates of 5, 10, 20, and 30 °C min^{-1}, respectively. From these results it can be suggested that the drying temperature is in the range of 100–125 °C and the processing temperature obtains a valuable material (composite) which can be controlled below 230 °C irrespective of heating rate. Among these three phases, phase II showed the highest weight loss *i.e.* the rate of mass loss was much faster and higher during devolatilization of PFs. It is also widely accepted that devolatilization of biomass through pyrolysis is useful in understanding multicomponent and multi-pyrolytic phases for process design, optimization and scale up.[64,65] Heating rate seems to be the critical parameter as elevated heating rate leads the designated peaks to higher temperatures for PF which is highly dependent on residence time *i.e.* high heating rate has low residence time. At high residence time, thermal gradient penetrates into the inner core of the particles and spreads out evenly, hence shows less dominant peak in the DTG plots (Fig. 6b). Conversion (α), range from 0 to 1, *vs.* temperature was also plotted for different heating rates, sigmoid shape profiles were obtained indicating that for the given value of α, the temperature increases with heating rates (Fig. 6c).

3.4.3 Kinetic study. Activation energy (E) is the energy required for the reaction to occur, and it is a vital kinetic parameter which can be determined by various model-fitting and model-free (iso-conversional) methods. Each method carries its own merits, and they are not in competition but are complementary. Iso-conversional model free methods can be either integral or differential and performed the kinetic analysis without having a specified reaction mechanism. On contrary, model-fitting approach uses the methodology of best fitting of the data to evaluate the $f(\alpha)$, E, and k_0. In this study, two iso-conversional model-free methods are used *i.e.* Friedman (differential) and KAS (integral), approaches to estimate E values. These methods are selected for the determination of kinetic parameters as they are accurate, most commonly and widely used methods. Coats–Redfern model, a model-fitting

method, is used to determine the reaction mechanism involved during the process.[25,61,62,66,67] Based on both iso-conversional methods (differential and integral), Arrhenius plots were established using data at different conversions from 0.1 to 0.9 with step size of 10% for OPT2-ads and parent PF samples (Fig. 7).

E values were obtained from the slope of linear regression lines for each conversion value as shown in Fig. 7a–d. Fig. 7a and c are the activation plots of OPT2-ads for E values calculation using KAS and Friedman methods, respectively. The mathematical forms of these aforementioned models are provided in the ESI† (mathematical forms of different models). R^2 was used to assess the quality of regression isoconversional models. The expressions of the regression models and their respective values of R^2 are provided in Table S5.† For OPT2-ads, the E values obtained from the KAS and Friedman methods are 180.24 kJ mol^{-1} and 205.61 kJ mol^{-1}, respectively. Using both methods, the average values of E of parent PF were 144.48 kJ mol^{-1} and 154.39 kJ mol^{-1} from KAS and Friedman, respectively (Fig. 7b and d). For both cases, the E value from the Friedman method was slightly higher than that from the KAS method. The high E value of OPT2-ads sample can be attributed to the increased bond energy resulting from the THF pre-treatment and metal adsorption, which consecutively enhances the thermal stability of the OPT2-ads compared to the parent PF.[68] Fig. 7e also shows the variations of E values with respect to conversion for both OPT2-ads and parent PF samples. The fluctuations in E values may be due to the complex multi-step reactions which include parallel, continuous and competitive reactions that occur during process.[55] Additionally, the variations in E values with conversions showed a similar trend for both methods: E was low at a low conversion value of 0.1, then steadily increased until a conversion of 0.7, followed by a sudden increase at the higher conversion range (0.7–0.9). In contrast, the same trends were observed for the parent PF sample using both models, but no sudden increase was observed at the higher conversion range (0.7–0.9). An increase in E value indicated endothermicity, while a decrease in E value was attributed to the exothermic reactions involved during PF pyrolysis in this conversion range[25,65] indicating no exothermic reactions involved during pyrolysis in both samples. The sudden increase in E value at the higher conversion range (0.7–0.9) for OPT2-ads could be due to the non-uniformity in the non-isothermal kinetic data, possibly caused by the adsorbed metals on the surface of the biosorbent or the formation of more unstable radicals joining simultaneously at a higher conversion range.[69,70] The non-uniformity (high error bars) in the data is evident from the R^2 values shown in Table S5† for the KAS and Friedman methods at 0.1 and 0.9 conversion values for the OPT2-ads sample and at 0.1, 0.8, and 0.9 conversion values for the parent PF sample. More uniform and consistent values with higher R^2 can be seen for the conversion range of 0.2–0.8 for OPT2-ads and 0.2–0.7 for PF, which confirms the presence of parallel straight lines with extremely slight variation in the same conversion range, as seen from the plot in Fig. 7a–d. This could be ascribed to similar kinetic behavior due to the same reaction mechanism.[71]
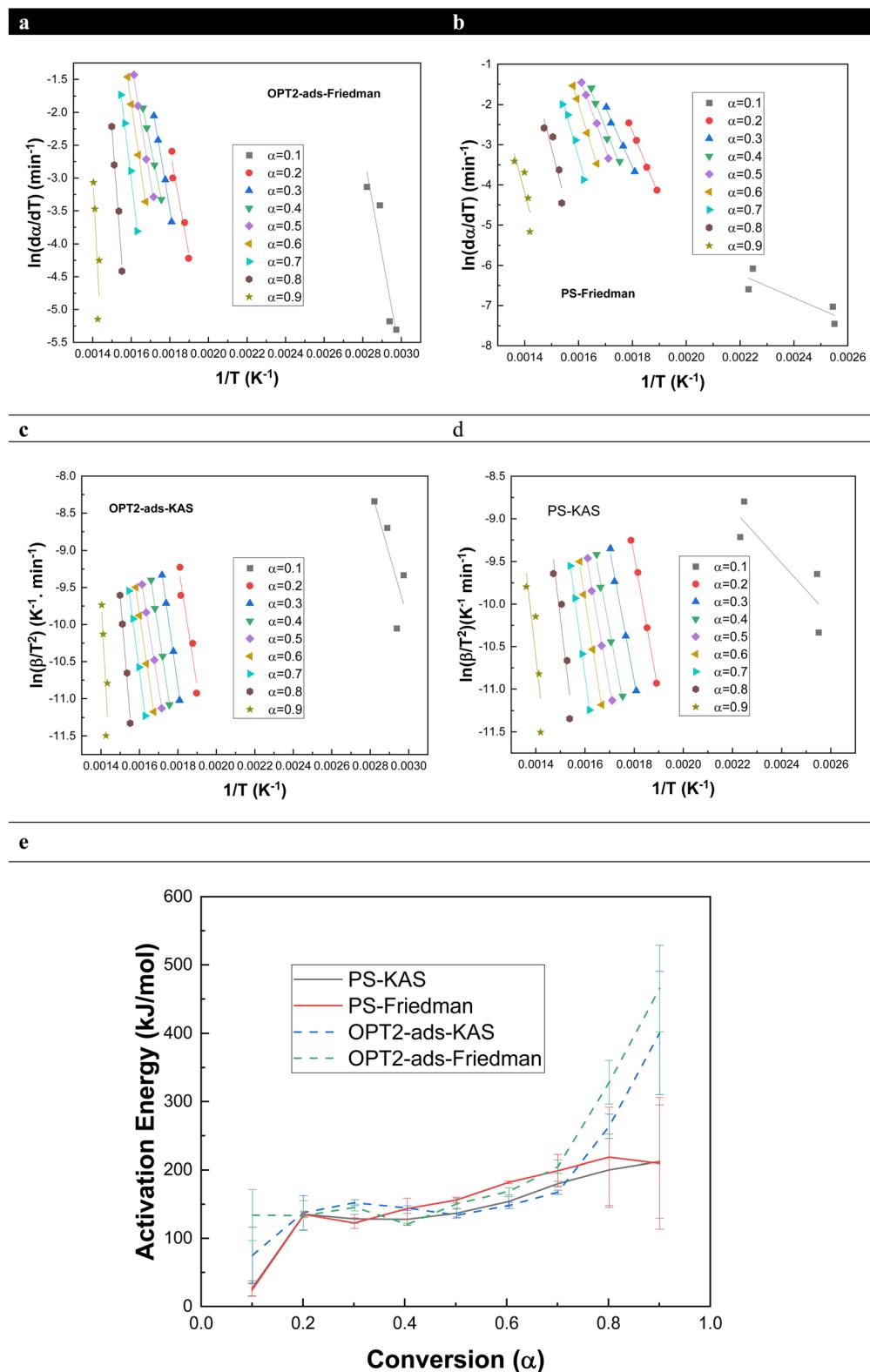
Fig. 7 Activation plots (a) Friedman plot for OPT2-ads (b) Friedman plot for the parent PF (c) KAS plot for OPT2-ads (d) KAS plot for the parent PF (e) variations in E vs. conversion for OPT2-ads and the parent PF samples.

On comparing with other materials reported in literature, Munagala et al.[28] determined the E value of CF for a limited range of fractions from 0.15–0.7 and they calculated the average values of 210.65 kJ mol^{-1}, 201.91 kJ mol^{-1}, and 200.94 kJ mol^{-1} using FWO, Starink and KAS methods respectively, which is very close to the E value of OPT2-ads sample. Kim et al.[72] analyzed

two types of chicken litter, flock and broiler, reporting E values of 484 kJ mol^{-1} and 464 kJ mol^{-1}, respectively, for 80% conversion. Recently, Khan et al.[73] determined the E value of a composite i.e. CF fiber reinforced poly-lactic acid for a temperature of 140–400 °C. The obtained E (112.06 kJ mol^{-1}) was observed to be well below our reported value. Chandrasekaran etal.[74] reported the E values of Prosopis Juliflora using two different integral methods i.e. KAS and FWO methods and calculated the values of 204.0 kJ mol^{-1} and 203.2 kJ mol^{-1}, respectively, which are also very close to OPT2-ads value. E values of some lignocellulosic biomasses such as wheat straw (379 kJ mol^{-1}), corn stover (240.6 kJ mol^{-1}) and corn stack (238 kJ mol^{-1}) were also calculated which were higher than E values obtained for OPT2-ads and parent PF samples.[75,76] Waste tires (239 kJ mol^{-1}) and waste plastic (235 kJ mol^{-1}) also found with higher E values compared to our samples.[77,78] The lower E value of natural fibers, ranging from 155 to 197 kJ mol^{-1}, is close to that of the parent PF, while the upper value approaches that of the OPT2-ads sample.[79] E values found in our study for PFs were also compared with the E values of other biomasses reported in literature (Table S6†) and they are in the range or close to most of the materials (biomass, natural fibers, plastic and tires etc.). For OPT2-ads, the values of R^2 from both models are close to unity, particularly in the conversion range of 0.2–0.8 attributing that both models mimic the experimental data well to determine E values.

3.4.4 Evaluation of reaction mechanism. As iso-conversional methods do not discuss the response of reaction mechanism, so Coats–Redfern model, a model fitting method, is used to determine the reaction mechanism involved during the process.[25,61,62,65–67] Expressions of different reaction mechanisms associated with the solid-state reactions are provided in ESI† (Fig. S1). In general, solid-state reactions involve phase boundary, diffusion (mass transport), nucleation and growth nuclei reactions. Coats–Redfern model equation was used for all different reaction mechanisms at heating rate of 10 °C min^{-1} to obtain apparent E, k_0 values and to predict the reaction mechanism for OPT2-ads sample. Overall E values and the E values for each phase (I, II, III) along with thermodynamic parameters for all reaction mechanisms are presented in Table 8. On comparing overall E values for different reaction mechanisms, E values are ranged from 20.54 to 34.18 kJ mol^{-1} for chemical reaction, 26.98 to 35.02 kJ mol^{-1} for diffusion reaction, 13.49 to 17.51 kJ mol^{-1} for phase interfacial reaction and 7.02–10.27 kJ mol^{-1} for nucleation and growth nuclei reaction. Among all the kinetic reaction models, diffusion models exhibited the highest E values for the mechanisms involved in diffusion. Based on the E values from all reaction mechanisms, the multi-dimensional diffusion model, specifically the three-dimensional diffusion-Jander (TDJ) model, is the rate-determining step for OPT2-ads. Not only was the overall E value high for the TDJ model, but the E values in every phase were also high, indicating that TDJ is the rate-determining step for each phase as well. Using the TDJ model, the overall E value for the parent PF sample was also calculated to be 39.45 kJ mol^{-1}. These results align completely with the literature for other biomasses, such as mustard stalk.[25] The pre-

exponential factor (k_0) was also determined using the Coats–Redfern method for all mechanism models at a constant heating rate of 10 °C min^{-1} for each phase (Table 8). Typically, k_0 is associated with the frequency of molecular collisions occurring in the correct orientation to trigger a reaction.[80] It was observed that k_0 decreased as the conversion progressed from lower ranges (phase II) to higher ranges (phase III). However, it remained consistent across all heating rates, with the estimated range for the selected TDJ model being 1.6×10^6 to 1.37×10^7 min^{-1}. For the same mechanism, the estimated k_0 values were 7.03×10^3 min^{-1} for phase I, 2.48×10^{11} min^{-1} for phase II, and 3.04×10^5 min^{-1} for phase III. A lower value ($<10^7$) of k_0 attributes that either reaction is surface dependent or a closed complex reaction while a higher k_0 values ($\geq 10^9$) may indicate a surface reaction transitioning to a more complex reaction, reflecting the increasing complexity of thermal degradation processes.[25,28]

3.5 Thermodynamic study

Numerous thermodynamic parameters, such as $\Delta G^{\neq}$, $\Delta H^{\neq}$, and $\Delta S^{\neq}$, were determined using basic thermodynamic relations provided in the ESI,† with their results presented in Table 8 for OPT2-ads. $\Delta G^{\neq}$ is a positive value that represents the free energy barrier for the formation of the activated complex. The activation enthalpy ($\Delta H^{\neq}$) is a state function, representing the heat absorbed or released at constant pressure.[80] $\Delta S^{\neq}$, the entropy of activation, is calculated using the values of $\Delta G^{\neq}$ and $\Delta H^{\neq}$. Table 8 presents these thermodynamic parameters for different phases as well as for the overall process of each mechanism at a heating rate of 10 °C min^{-1}, calculated using the Coats–Redfern method. According to Table 8, the highest values of $\Delta G^{\neq}$ and $\Delta H^{\neq}$ come from two diffusion models, TDJ and TDGB. The values of $\Delta G^{\neq}$ and $\Delta H^{\neq}$ are similar for both models; however, TDJ was selected due to its higher R^2 values, and it had already been identified as the rate-determining step as discussed earlier. For each model and the overall process, $\Delta S^{\neq}$ is negative, indicating that the disorder of the products, resulting from bond dissociation, is less than that of the initial reactants. Based on the TDJ mechanism, $\Delta G^{\neq}$, $\Delta H^{\neq}$, and $\Delta S^{\neq}$ were also calculated for the parent PF (both overall and for each phase), and for these values, $\Delta G^{\neq}$ and $\Delta H^{\neq}$ were positive and $\Delta S^{\neq}$ was negative. Furthermore, based on the TDJ reaction mechanism, these thermodynamic properties were obtained at varying α values (0.1–0.9) for both OPT2-ads and the parent PF, using both iso-conversional methods, as presented in Fig. 8. Fig. 8a and b shows the $\Delta H^{\neq}$ values varying with α values (0.1–0.9) for both OPT2-ads and parent PF at two different heating rates (10 and 20 °C min^{-1}). For both samples, all $\Delta H^{\neq}$ values were close across different heating rates, indicating a negligible effect of heating rates on $\Delta H^{\neq}$ values. This minor impact on $\Delta H^{\neq}$ signifies the energy difference between reagents and the activated complex.[25] Furthermore, the $\Delta H^{\neq}$ values for both samples are positive, with the highest values of $\Delta H^{\neq}$ at high conversion values—0.9 for both samples. This difference in $\Delta H^{\neq}$ at higher conversion is due to non-uniformity as previously explained. Positive values indicate strong bonds between

Table 8 Evaluation of overall and for each phase (I, II, III) E values along with thermodynamic parameters to predict reaction mechanisms of OPT2-ads at heating rate of 10 °C min^{-1} using Coats–Redfern method

Mechanism	Phases	E (kJ mol^{-1})	k_0 (min^{-1})	$\Delta G^{\neq}$ (kJ mol^{-1})	$\Delta H^{\neq}$ (kJ mol^{-1})	$\Delta S^{\neq}$ (kJ mol^{-1} K^{-1})	R^2
OD	Overall	26.98 ± 0.47	1.47 × 10^6	129.20	21.89	−0.175	0.8907
	Phase 1	17.65 ± 1.40	4.88 × 10^4	137.24	12.55	−0.203	0.5180
	Phase 2	68.26 ± 1.10	1.70E+10	122.81	63.13	−0.097	0.9809
	Phase 3	5.340 ± 0.15	1.30 × 10^4	131.68	0.250	−0.214	0.8793
TD	Overall	30.10 ± 0.51	2.21 × 10^6	130.27	25.01	−0.172	0.8970
	Phase 1	17.88 ± 1.40	3.62 × 10^4	138.99	12.79	−0.206	0.5218
	Phase 2	77.34 ± 1.00	7.59E+10	124.31	72.25	−0.085	0.9874
	Phase 3	9.530 ± 0.20	2.89 × 10^4	131.78	4.440	−0.208	0.9272
TDJ	Overall	35.02 ± 0.57	2.61 × 10^6	134.35	29.93	−0.170	0.9020
	Phase 1	18.13 ± 1.44	7.03 × 10^3	147.59	13.04	−0.220	0.5257
	Phase 2	88.72 ± 0.86	2.48 × 10^{11}	129.66	83.63	−0.075	0.9930
	Phase 3	21.77 ± 0.23	3.04 × 10^5	132.03	16.68	−0.188	0.9812
TDGB	Overall	31.65 ± 0.53	8.35 × 10^5	136.78	26.56	−0.180	0.8996
	Phase 1	17.96 ± 1.43	6.44 × 10^3	147.87	12.87	−0.220	0.5231
	Phase 2	81.09 ± 0.96	4.10E+10	131.19	76.00	−0.090	0.9897
	Phase 3	12.96 ± 0.21	2.63 × 10^4	135.71	7.870	−0.209	0.9567
FOR	Overall	20.54 ± 0.35	1.46 × 10^6	122.80	15.45	−0.175	0.8969
	Phase 1	9.190 ± 0.72	1.99 × 10^4	133.33	4.100	−0.211	0.5295
	Phase 2	50.44 ± 0.37	1.08 × 10^9	119.07	45.35	−0.120	0.9959
	Phase 3	20.64 ± 0.29	1.87 × 10^6	121.64	15.55	−0.173	0.9644
SOR	Overall	34.18 ± 0.80	1.45 × 10^8	113.05	29.09	−0.137	0.8191
	Phase 1	9.570 ± 0.73	2.49 × 10^3	132.58	4.480	−0.209	0.5407
	Phase 2	72.55 ± 0.61	2.09 × 10^{11}	114.34	67.46	−0.077	0.9947
	Phase 3	76.84 ± 2.20	3.34 × 10^{11}	116.26	71.75	−0.073	0.8723
ODPIR	Overall	13.49 ± 0.24	1.09 × 10^5	128.97	8.400	−0.197	0.8907
	Phase 1	8.820 ± 0.71	1.61 × 10^4	134.07	3.730	−0.213	0.5180
	Phase 2	34.11 ± 0.55	1.86 × 10^7	123.41	29.02	−0.154	0.9809
	Phase 3	2.670 ± 0.07	4.57 × 10^3	134.33	−2.420	−0.223	0.8793
TDPIR	Overall	16.28 ± 0.27	1.58 × 10^5	129.88	11.19	−0.194	0.9009
	Phase 1	9.000 ± 0.72	8.96 × 10^3	137.23	3.910	−0.218	0.5237
	Phase 2	41.56 ± 0.46	6.10 × 10^7	124.83	36.47	−0.144	0.9908
	Phase 3	7.330 ± 0.10	2.37 × 10^4	130.99	2.640	−0.209	0.9699
TrDPIR	Overall	17.51 ± 0.29	1.65 × 10^5	130.88	12.42	−0.193	0.9020
	Phase 1	9.060 ± 0.72	6.19 × 10^3	139.18	3.970	−0.221	0.5257
	Phase 2	44.36 ± 0.43	8.12 × 10^7	126.17	39.27	−0.142	0.9930
	Phase 3	10.88 ± 0.11	4.46 × 10^4	130.93	5.790	−0.204	0.9812
TDNGR	Overall	10.27 ± 0.17	9.52 × 10^4	126.46	5.180	−0.198	0.8969
	Phase 1	4.590 ± 0.36	7.43 × 10^3	133.78	−0.500	−0.219	0.5295
	Phase 2	25.21 ± 0.19	4.04 × 10^6	122.31	20.12	−0.167	0.9959
	Phase 3	10.32 ± 0.15	1.07 × 10^5	125.87	5.230	−0.197	0.9644
TrDNGR	Overall	7.020 ± 0.12	3.29 × 10^4	128.62	1.930	−0.207	0.8969
	Phase 1	4.020 ± 0.24	5.89 × 10^3	134.39	−1.070	−0.221	0.5295
	Phase 2	16.89 ± 0.12	5.30 × 10^5	124.34	11.80	−0.184	0.9959
	Phase 3	7.870 ± 0.15	4.01 × 10^4	128.48	2.780	−0.205	0.9644
TDJ-parent PF	Overall	39.45 ± 0.57	5.94 × 10^6	133.25	34.43	−0.163	0.9229
	Phase 1	24.35 ± 1.57	3.19 × 10^4	144.42	19.33	−0.207	0.6304
	Phase 2	94.59 ± 0.78	8.24 × 10^{11}	128.87	89.56	−0.065	0.9951
	Phase 3	22.39 ± 0.21	3.41 × 10^5	130.55	17.37	−0.187	0.9850

the bio-sorbent and trace metals due to the formation of an activated complex, attributed to low potential energy. Additionally, the positive $\Delta H^{\neq}$ values confirm that the pyrolysis process of PFs is endothermic. Fig. 8c and d also shows the $\Delta G^{\neq}$ with conversion for OPT2-ads and parent PF at 10 and 20 °C min^{-1} heating rates, where it shows almost the same pattern as $\Delta H^{\neq}$ as maximum value achieved at 0.9 for both samples. These positive $\Delta G^{\neq}$ values indicate that pyrolysis of PFs is non-spontaneous, energy-intensive, and thermodynamically unfavorable. These values are within the range reported for other biomasses in the literature, suggesting that PF has potential as a bioenergy feedstock.[81–83] For instance, the obtained average $\Delta G^{\neq}$ values of OPT2-ads (KAS: 190.99 kJ mol^{-1} and Friedman: 192.24 kJ mol^{-1}) and parent PF (KAS: 195.06 kJ mol^{-1} and Friedman: 233.92 kJ mol^{-1}) at a heating rate of 10 °C min^{-1} are higher than coffee silver skin biomass (173.22 kJ mol^{-1}),[81] mustard stalk (127.74 kJ mol^{-1}),[25] maize (162.83 kJ mol^{-1}),[82] and close to Azadirachta indica

10 °C min⁻¹ 20 °C min⁻¹
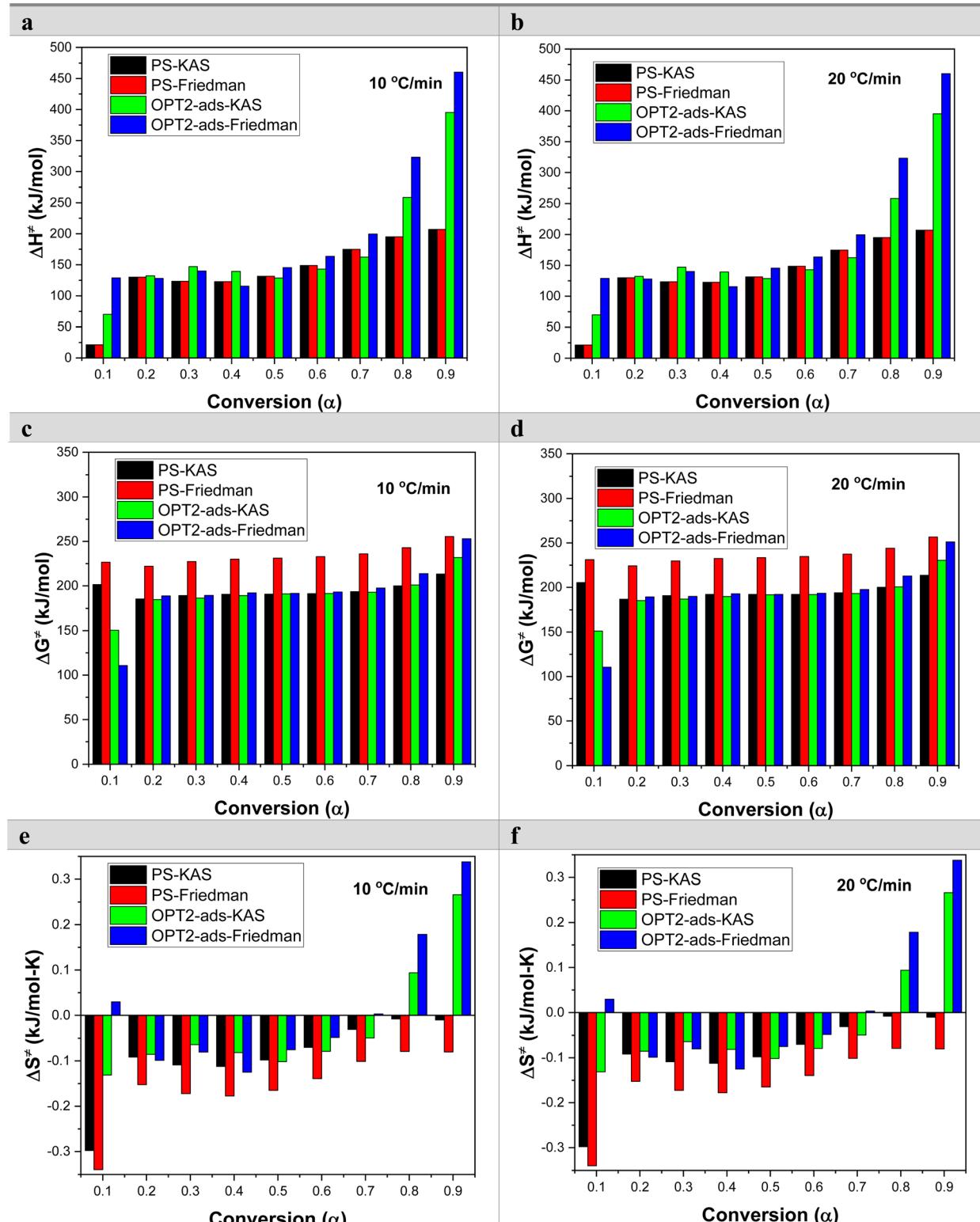
Fig. 8 $\Delta H^{\neq}$ vs. conversion for OPT2-ads and the parent sample (a) 10 °C min⁻¹ (b) 20 °C min⁻¹; $\Delta G^{\neq}$ vs. conversion for OPT2-ads and the parent sample (c) 10 °C min⁻¹ (d) 20 °C min⁻¹; $\Delta S^{\neq}$ vs. conversion for OPT2-ads and the parent sample (e) 10 °C min⁻¹ (f) 20 °C min⁻¹

(215.42 kJ mol⁻¹).[83] Additionally, $\Delta S^{\neq}$ represents the closeness of a system to its thermodynamic equilibrium. The variations of $\Delta S^{\neq}$ with conversions are shown in Fig. 8e and f for both OPT2-

ads and parent PF. All $\Delta S^{\neq}$ values were negative for parent sample however, for OPT2-ads the values were negative until 0.7 conversion and then turned positive at higher conversion

values. Low $\Delta S^{\neq}$ values indicate a low degree of disorder. Consequently, PF only underwent some physical and chemical changes until it reached a state close to its thermodynamic equilibrium.[84] High entropy values indicated a comparatively high degree of disorder and reactivity, suggesting the formation of an activated complex generally occurs when high entropy is observed.[57b] The parametric values at different heating rates (5, 10, 20, and 30 °C min^{-1}) for the OPT2-ads sample, using the Coats–Redfern method for all reaction mechanisms, were also obtained and are presented in the ESI† (Table S7). Table S8† shows that all $\Delta G^{\neq}$ and $\Delta H^{\neq}$ values are positive, with no significant variation observed as the heating rates change. Likewise, the values of $\Delta S^{\neq}$ exhibit no substantial differences, although all $\Delta S^{\neq}$ values are negative. Furthermore, the average values of thermodynamic parameters calculated using Friedman ($\Delta G^{\neq}$: 192.24 kJ mol^{-1} @ 10 °C min^{-1}) and KAS ($\Delta G^{\neq}$: 190.99 kJ mol^{-1} @ 10 °C min^{-1}) methods were substantially close to each other. However, the high standard deviation values for the results of the iso-conversional methods were caused by the results of Friedman method ($\sigma_{\Delta G^{\neq}}$: ±36 kJ mol^{-1}; $\sigma_{\Delta H^{\neq}}$: ±116 kJ mol^{-1}; $\sigma_{\Delta S^{\neq}}$: 0.152 kJ mol^{-1} K^{-1}) compared to KAS method ($\sigma_{\Delta G^{\neq}}$: ±20 kJ mol^{-1}; $\sigma_{\Delta H^{\neq}}$: ±96 kJ mol^{-1}; $\sigma_{\Delta S^{\neq}}$: 0.126 kJ mol^{-1} K^{-1}), probably due to the noise caused by experimental error and/or the intrinsic inaccuracy of the differential methods (Friedman), which can be particularly encountered for non-isothermal kinetic data obtained by means of TGA.[85] Overall, kinetic and thermodynamic parameters indicate that the maximum reaction rate occurs at high conversion values for both samples. Furthermore, they also suggest that PFs have the potential to act as a bioenergy feedstock.

4 Conclusions

The study focused on optimizing the removal of six heavy metals (V^{5+}, As^{3+}, Cr^{6+}, Co^{2+}, Ni^{2+}, Cd^{2+}) from MMSW using two different statistical approaches. The first optimization used RSM with BBD while the second used CCD. The study evaluated different independent variables and their effects on metal removal efficiency, finding high accuracy in predictive models based on different performance indicators R^2, RMSE, MAE and RE. Single and multi-objective optimizations along with desirability functions were performed, showing that two-step optimization improved metal removal efficiencies, except for Cr^{6+}. In the ANOVA analysis, the PF : THF ratio was the most significant factor in the first optimization, while in the second optimization, both PF dose and biosorption time were significant, with PF dose being more influential.

The study further analyzed the spent and parent PFs for thermal decomposition, physicochemical properties, and both thermodynamic ($\Delta H^{\neq}$, $\Delta G^{\neq}$, $\Delta S^{\neq}$) and kinetic parameters (E, A) using TGA data at different heating rates (5–30 °C min^{-1}). Spent PF showed a higher E compared to the parent PF using both iso-conversional methods. The TDJ model was determined as the rate-determining step for the thermal degradation of spent as well as parent PFs using Coats–Redfern model. Thermodynamic analysis indicated that maximum reaction rates occurred at

high conversion values for both spent and parent PFs. Overall, these physicochemical, kinetic, and thermodynamic properties suggest that PFs are promising as biofuels and for other valuable applications.

Biosorption for removing multiple metals is complex, necessitating advanced biosorbents to adsorb all trace metals effectively. Thus, further research is required to develop efficient biosorbents through cost-effective treatments that enhance their surface and chemical properties. Refining current predictive models or leveraging artificial intelligence can expand biosorption's use in water remediation, reducing experimental demands. Future research should focus on the scalability and practical applicability of these models, combining biosorption with advanced technologies like membrane systems to address high costs and enhance sustainability. A circular economic approach emphasizes reusing waste, such as blending spent biosorbents with other materials, to create value-added products. This research lays the groundwork for sustainable, cost-effective energy production and water treatment solutions using waste and biosorbents.

Abbreviation

THF	Tetrahydrofuran
PF	Poultry feather
OPT2-ads	Spent biosorbent *i.e.* THF treated sample after biosorption at optimum 2 conditions
RSM	Response surface methodology
BBD	Box–Behnken Design
CCD	Central composite design
KAS	Kissinger-Akahira-Sunose
MMSW	Multi-metals simulated water
OSPW	Oil sand process-affected water
y	Percent removal efficiency (dependent variable) (%)
x_i, x_j	Coded variables
β_0	Model intercept
β_i	Linear coefficient
β_{ii}	Quadratic coefficient
β_{ij}	Cross interaction coefficient
N	No of independent factors
ε	Error
R^2	Coefficient of determination
RMSE	Root mean square error
MAE	Mean absolute error
RE	Percent relative error (%)
ANOVA	Analysis of variance
OF	Objective function
A	Pretreatment process temperature (°C)
B	Pretreatment process time (min)
C	PF : THF ratio (g ml^{-1})
X	Modified biosorbent dose (g)
Y	Biosorption process time (h)
OFAT	One-factor-at-a-time
M1	Predicted values of Optimization-1 (%)
M2	Predicted values of Optimization-2 (%)
$\dfrac{d\alpha}{dt}$	Conversion rate (s^{-1})

$k(T)$	Rate constant (s^{-1})
k_0	Pre-exponential factor (s^{-1})
E	Activation energy (J mol^{-1})
R	Universal gas constant (J mol^{-1}. K^{-1})
$\Delta H^{\neq}$	Enthalpy of activation (J mol^{-1})
$\Delta G^{\neq}$	Gibbs energy of formation for activation complex (J mol^{-1})
$\Delta S^{\neq}$	Entropy of activation (J mol^{-1} K^{-1})
β	Heating rate (°C min^{-1})
$g(\alpha)$	Integral reaction mechanism function
$f(\alpha)$	Differential reaction mechanism function
d	Individual desirability function
D	Composite desirability function
TGA	Thermogravimetric analysis (wt%)
DTG	Derivative thermogravimetric (wt% °C^{-1})
FC	Fixed carbon (wt%)
MC	Moisture content (wt%)
VM	Volatile matter (wt%)

Data availability

Data will be made available upon reasonable request from corresponding author.

Conflicts of interest

There are no conflicts to declare.

Acknowledgements

Notes and references

1 A. Haghighizadeh, O. Rajabi, A. Nezarat, Z. Hajyani, M. Haghmohammadi, S. Hedayatikhah, S. D. Asl and A. A. Ben, *Arabian J. Chem.*, 2024, **17**, 105777.
2 P. Sharma, D. Dutta, A. Udayan and S. Kumar, *J. Environ. Chem. Eng.*, 2021, **9**, 106673.
3 I. Zahara, M. F. Irfan, M. Zubair, T. Siddique and A. Ullah, *Sci. Total Environ.*, 2023, **891**, 164288.
4 S. R. Dhokpande, S. M. Deshmukh, A. Khandekar and A. Sankhe, *Sep. Purif. Technol.*, 2024, **350**, 127868.
5 M. W. Nugraha, S. Kim, F. Roddick, Z. Xie and L. Fan, *J. Water Process Eng.*, 2025, **70**, 106960.
6 A. Kumar, S. Sidharth and B. Kandasubramanian, *Environ. Sci. Pollut. Res.*, 2023, **30**, 39474–39493.
7 Y. Wen, C. Xue, D. Ji, Y. Hou, K. Li and Y. Li, *Colloids Surf., A*, 2023, **656**, 130531.
8 N. Sultana, S. M. Z. Hossain, M. E. Mohammed, M. F. Irfan, B. Haq, M. O. Faruque, S. A. Razzak and M. M. Hossain, *Sci. Rep.*, 2020, **10**, 15068.
9 M. F. Irfan, S. M. Z. Hossain, I. Tariq, N. A. Khan, A. Tawfeeqi, A. Goeva and M. Wael, *Min., Metall., Explor.*, 2020, **37**, 1367–1383.
10 M. F. Irfan, S. M. Z. Hossain, H. Khalid, F. Sadaf, S. Al-Thawadi, A. Alshater, M. M. Hossain and S. A. Razzak, *Biotechnol. Rep.*, 2019, **23**, e00356.
11 M. Ans, M. A. Makhdoom, M. F. Irfan and A. Al-Abir, *Miner. Eng.*, 2022, **175**, 107279.
12 C. Yang, C. Jiang, Y. Fu, F. Chen and J. Hu, *J. Mol. Liq.*, 2022, **345**, 118251.
13 E. C. Umejuru, E. Prabakaran and K. Pillay, *ACS Omega*, 2021, **6**, 11155–11172.
14 Z. Chen, R. Zheng, W. Wei, W. Wei, W. Zou, J. Li, B. J. Ni and H. Chen, *Resour., Conserv. Recycl.*, 2022, **178**, 106037.
15 M. W. Mofulatsi, E. Prabakaran, T. Velempini, E. Green and K. Pillay, *Microporous Mesoporous Mater.*, 2022, **329**, 111480.
16 B. Verbinnen, C. Block, J. Van Caneghem and C. Vandecasteele, *Waste Manage.*, 2015, **45**, 407–411.
17 V. K. Rathore and P. Mondal, *J. Environ. Manage.*, 2017, **200**, 160–169.
18 W. Tao, L. Qi, H. Duan and S. Liu, *Water Sci. Technol.*, 2017, **75**, 1812–1819.
19 D. D. Ngobeni, MSc. (Chemistry) Dissertation, University of Johannesburg, 2019, Retrieved from **https://ujcontent.uj.ac.za**.
20 E. Martinez-Hernandez, J. Sadhukhan, J. Aburto, A. Myriam, M. Stephen and M. Richard, *Clean Technol. Environ. Policy*, 2022, **24**, 1709–1725.
21 X. Guo and C. Liu, *Thermochim. Acta*, 2024, **738**, 179802.
22 R. A. Alsulami, S. A. El-Sayed, M. A. Eltaher, A. Mohammad, K. H. Almitani and M. E. Mostafa, *Fuel*, 2023, **334**, 126600.
23 M. E. Mostafa and S. A. El-Sayed, *Energy*, 2025, **330**, 136823.
24 O. Bongomin, C. Nzila, J. Igadwa Mwaslagi and O. Maube, *Energy Convers. Manage.*, 2024, **24**, 100723.
25 K. Patidar, A. Singathia, M. Vashishtha, V. K. Sangal and S. Upadhyaya, *Mater. Sci. Energy Technol.*, 2022, **5**, 6–14.
26 T. Rasool, V. C. Srivastava and M. N. S. Khan, *Process Integr. Optim. Sustain.*, 2018, **2**, 259–268.
27 H. Li, J. Hu, Y. Meng, J. Su and X. Wang, *Sci. Total Environ.*, 2017, **603–604**, 39–48.
28 C. K. Munagala, N. Kathula, S. M. D. Razak, A. K. Kesari, H. Nagar, S. Bojja and H. Aniya, *Biomass Convers. Biorefin.*, 2022, **14**, 27647–27670.
29 E. Senoz and R. P. Wool, *Int. J. Hydrogen Energy*, 2011, **36**, 7122–7127.
30 Z. Zhao, Y. Wang, M. Li and R. Yang, *RSC Adv.*, 2015, **5**, 34803–34811.
31 I. Zahara, M. F. Irfan, T. Siddique and A. Ullah, *J. Water Process Eng.*, 2025, **75**, 107891.
32 M. N. Chollom, S. Rathilal, F. M. Swalaha, B. F. Bakare and E. K. Tetteh, *Environ. Eng. Res*, 2020, **25**, 114–122.
33 S. M. Z. Hossain, N. Sultana, M. F. Irfan and S. A. Razzak, *Int. J. Energy Res.*, 2022, **46**, 20519.
34 S. M. Z. Hossain, S. Taher, A. Khan, N. Sultana, M. F. Irfan, B. Haq and S. A. Razzak, *Arabian J. Sci. Eng.*, 2020, **45**, 7371–7383.
35 F. Mumtaz, M. F. Irfan, W. A. Butt and M. R. Usman, *Int. J. Environ. Sci. Technol.*, 2023, **20**, 7149–7166.
36 T. Tesfaye, B. Sithole, D. Ramjugernath and V. Chunilall, *Waste Manage.*, 2017, **68**, 626–635.

37 C. C. Y. Ling and S. F. Y. Li, *J. Hazard. Mater.*, 2023, **455**, 131600.

38 T. A. Mamvura and G. Danha, *Heliyon*, 2020, **6**, e03531.

39 M. F. Irfan, S. M. Z. Hossain, M. Ans, B. S. Al-Anzil and A. Ullah, *Int. J. Environ. Sci. Technol.*, 2025, **22**, 7753.

40 J. A. Raven and R. J. Geider, *New Phytol.*, 1988, **110**, 441–461.

41 J. C. Igwe and A. A. Abia, *Ecletica Quim.*, 2007, **32**, 33–42.

42 C. Anyika, N. A. M. Asri, Z. A. Majid, J. Jaafar and A. Yahya, *Appl. Water Sci.*, 2017, **7**, 4573–4591.

43 A. A. Okoya, N. O. Ochor, A. B. Akinyele and O. O. Olaiya, *J. Agric. Ecol. Res. Int.*, 2020, **21**, 43–53.

44 R. Chakraborty, A. Asthana, A. K. Singh, S. Yadav, M. A. B. H. Susan and S. A. C. Carabineiro, *J. Mol. Liq.*, 2020, **312**, 113475.

45 E. Solgi and A. Zamanian, *Arch. Hyg. Sci.*, 2020, **9**, 97–108.

46 M. Moradi, H. Arabi and M. Shamsborhan, *Optik*, 2020, **202**, 163619.

47 A. Chabbi, M. A. Yallese, I. Meddour, M. Nouioua, T. Mabrouki and F. Girardin, *Measurement*, 2017, **95**, 99–115.

48 L. Tan, H. Wang, C. Yang and B. Niu, *Nat. Comput.*, 2017, **16**, 549–565.

49 M. F. Irfan, M. Ans, S. M. Z. Hossain, T. Siddique and A. Ullah, *J. Dispersion Sci. Technol.*, 2025, 1–18.

50 H. M. Hamadeen, E. A. Elkhatib and M. L. Moharem, *Sci. Rep.*, 2022, **12**, 14174.

51 R. Garg, R. Garg, M. Sillanpaa, M. Alimuddin, M. A. Khan, N. M. Mubarak and Y. H. Tan, *Sci. Rep.*, 2023, **13**, 6859.

52 H. A. Yusuf, S. M. Z. Hossain, A. A. Khamis, H. T. Radhi and A. S. Jaafar, *J. CO₂ Util.*, 2020, **42**, 101291.

53 L. He, Y. Chen, X. Wu, S. Chen, J. Liu and Q. Li, *Water*, 2020, **12**, 34.

54 N. Hossain, S. Nizamuddin, G. Griffin, P. Selvakannan, N. M. Mubarak and T. M. I. Mahlia, *Sci. Rep.*, 2020, **10**, 18851.

55 C. N. Arenas, M. V. Navarro and J. D. Martínez, *Bioresour. Technol.*, 2019, **288**, 121485.

56 S. Park, S. J. Kim, K. C. Oh, L. H. Cho, Y. K. Jeon, C. Lee and D. H. Kim, *Energy Rep.*, 2022, **8**, 12038–12044.

57 (*a*) R. K. Singh, D. Pandey, T. Patil and A. N. Sawarkar, *Bioresour. Technol.*, 2020, **310**, 123464; (*b*) R. K. Singh, T. Patil and A. N. Sawarkar, *Bioresour. Technol. Rep.*, 2020, **12**, 100558.

58 R. Tungal and R. V. Shende, *Appl. Energy*, 2014, **134**, 401–412.

59 H. Chen, X. Yang, Y. Liu, X. Lin, J. Wanga, Z. Zhang, N. Li, Y. Li and Y. Zhang, *Waste Manage.*, 2021, **130**, 82–92.

60 M. Dudynski, K. Kwiatkowski and K. Bajer, *Waste Manage.*, 2012, **32**, 685–691.

61 M. F. Irfan, A. Arami-Niya, M. H. Chakrabarti, W. M. A. Wan Daud and M. R. Usman, *Energy*, 2012, **37**, 665–672.

62 M. F. Irfan, M. H. Chakrabarti and K. Kusakabe, *Can. J. Chem. Eng.*, 2013, **91**, 1936–1944.

63 T. Tesfaye, B. Sithole, D. Ramjugernath and T. Mokhothu, *Sustainable Chem. Pharm.*, 2018, **9**, 27–34.

64 E. Ranzi, P. E. A. Debiagi and A. Frassoldati, *ACS Sustain. Chem. Eng.*, 2017, **5**, 2867–2881.

65 I. Ali and A. Bahadar, *Front. Energy Res.*, 2019, **7**, 1–14.

66 M. A. Farrukh, K. M. Butt, K. K. Chong and W. S. Chang, *J. Saudi Chem. Soc.*, 2019, **23**, 561–575.

67 S. Ramukutty, E. Ramachandran and J. Cryst, *Process. Technol.*, 2014, **4**, 71–78.

68 S. Oza, H. Ning, I. Ferguson and N. Lu, *Composites, Part B*, 2014, **67**, 227–232.

69 S. Hooda, R. Lanjewar and P. Mondal, *J. Energy Inst.*, 2023, **108**, 101247.

70 S. Yousef, J. Eimontas, N. Striugas and M. A. Abdelnaby, *J. Anal. Appl. Pyrolysis*, 2021, **156**, 5360–5374.

71 L. Wang, H. Lei, J. Liu and Q. Bu, *RSC Adv.*, 2018, **8**, 2196–2202.

72 S. S. Kim and F. A. Agblevor, *Waste Manage.*, 2007, **27**, 135–140.

73 A. Khan, S. A. Alghamdi, A. S. Almuflih, A. Abdulrahman, K. M. Qureshi, N. Almakayeel and M. R. N. Qureshi, *Heliyon*, 2024, **10**, e24245.

74 A. Chandrasekaran, S. Ramachandran and S. Subbiah, *Bioresour. Technol.*, 2017, **233**, 413–422.

75 J. Cai, W. Wu, R. Liu and G. W. Huber, *Green Chem.*, 2013, **15**, 1331–1339.

76 L. Luo, X. Guo, Z. Zhang, M. Chai, M. M. Rahman, X. Zhang and J. Cai, *Energy Fuels*, 2020, **34**, 4874–4881.

77 H. Liu, C. Wang, J. Zhang, W. Zhao and M. Fan, *Energy Fuels*, 2020, **34**, 2385–2390.

78 T. Menares, J. Herrera, R. Romero, P. Osorio and L. E. Arteaga-Pérez, *Waste Manage.*, 2020, **102**, 21–29.

79 F. Yao, Q. Wu, Y. Lei, W. Guo and Y. Xu, *Polym. Degrad. Stab.*, 2008, **93**, 90–98.

80 I. Ali, R. Tariq, S. R. Naqvi, A. H. Khoja, M. T. Mehran, M. Naqvi and N. Gao, *J. Energy Inst.*, 2021, **95**, 30–40.

81 S. Pinzi, C. Buratti, P. Bartocci, G. Marseglia, F. Fantozzi and M. Barbanera, *Fuel*, 2020, **278**, 118260.

82 V. Zsinka, B. L. Tarcsay and N. Miskolczi, *Energies*, 2024, **17**, 1875.

83 G. de la Rosa, H. E. Reynel-Avila, A. Bonilla-Petriciolet, I. Cano-Rodríguez, C. Velasco-Santos and A. L. Martínez-Hernández, *World Acad. Sci. Eng. Technol.*, 2008, **47**, 394–402.

84 C. A. Solís-Moreno, E. Cervantes-Gonzále and M. Z. Saavedra-Leo, *J. Environ. Health Sci. Eng.*, 2021, **19**, 707–720.

85 K. Açıkalın and G. Gözke, *Bioresour. Technol.*, 2021, **342**, 125936.